

Sphere packings and local environments in Penrose tilings

C. L. Henley

AT&T Bell Laboratories, Murray Hill, New Jersey 07974
*and Department of Physics, Cornell University, Ithaca, New York 14853-2501**

(Received 13 January 1986)

Packings of spheres placed on vertices of two- or three-dimensional Penrose tilings arise in various models of glassy or "quasicrystal" metals. Such packings are described, with particular attention to the packing fractions and coordination numbers: In particular, one of the three-dimensional packings attains a packing fraction close to that of random close packing. The frequencies of various local environments are also enumerated. Relations between the tiling and density-wave pictures of icosahedral structures are clarified.

I. INTRODUCTION

A. Complicated structures and sphere packings

The recently discovered icosahedral alloys, $i(\text{Al-Mn})$ (Refs. 1 and 2) and $i(\text{Al-Zn-Mg})$ (Ref. 3) have diffraction patterns closely similar to that of the nonperiodic three-dimensional Penrose tiling (3D PT) (Refs. 4 and 5). This similarity has motivated attempts to guess the structure (i.e., atomic positions) using the 3D PT (or a set of icosahedral density waves) as a framework. These model structures⁶⁻¹⁵ are related, in various ways, to packings of space by identical spheres.

Such packings, with spheres representing atoms, have long been used to model complex metallic alloy phase structures,¹⁶ large noncrystallographic clusters^{17,18} and metallic liquids or glasses.¹⁹⁻²⁴ The spheres may interact with central forces ("soft spheres"); or, in massive simplification, repulsive and attractive parts of the interaction potential may be replaced by an impenetrable hard core of diameter D , plus an external pressure to ensure that the hard spheres are rigidly packed. Generally one is interested in (i) the packing fraction f (see below), which measures the density of the packing, and (ii) the distribution of local coordinations.

In this paper, I describe some efficient packings in which spheres are centered on special subsets of the vertices of Penrose tilings in two and three dimensions. Results are also presented on the frequency of various local environments in the Penrose tilings (independent of the spheres packed on them). This information is needed to compute the packing fraction and frequencies of local coordinations of the sphere packings, but it is likely to have wider applications.

It is proverbial that the "best" packing around a sphere by neighbors is icosahedral.¹⁶⁻²⁰ In recent years this notion has been developed systematically into a theory which describes the atomic arrangements of Frank-Kasper phases and metallic glasses in terms of defects with respect to an ideal icosahedrally coordinated network, which can actually be realized only in curved space.²¹⁻²⁴ It is important to note that Penrose tiling models⁷⁻¹⁴ are a *parallel* development to the curved-space

models. They have different, not necessarily related, kinds of icosahedral order, which may nevertheless be studied in a similar spirit. My investigation of the local coordinations of the Penrose tilings is parallel in this way to the study by Mosseri and Sadoc^{21,22} of local coordinations in the hierarchical packing of tetrahedra generated by the "iterative flattening" method.

In this paper, I have only considered how best to pack spheres, *given* that their centers lie on Penrose tiling vertices. I have not determined whether there exist conditions in which such a quasiperiodic packing might be more efficient than any periodic one. Hope for this possibility is *not* encouraged by the examples exhibited here (of which the quasiperiodic pentagon packing of Sec. II B A is the best attempt).

B. Definitions

A set of points $\{\mathbf{y}_i\}$ and diameters $\{D_i\}$ satisfying $|\mathbf{y}_i - \mathbf{y}_j| \geq (D_i + D_j)/2$ for all $i \neq j$ will be called a *sphere packing* (or disk packing, in two dimensions). Apart from one place (Sec. II B 5), I will only consider sets $\{\mathbf{y}_i\}$ which are subsets of the vertices of a Penrose tiling, and I will take the spheres (disks) to be identical, $D_i \equiv D$. The *packing fraction* f is the ratio of the occupied volume $\sum_i \pi D_i^3/6$ (or area $\sum_i \pi D_i^2/4$) to the total system volume (or area) in the infinite-system limit.

A notable feature of Penrose tilings is that there is a discrete set of possible site separations, say $\{r_1, r_2, r_3, \dots\}$ in ascending order (note Tables II and VI and Fig. 11, below). This means that the interesting sphere packings with centers $\{\mathbf{y}_i\}$ on sites of the tiling must have $D = r_n$ for some n . For if $r_{n-1} < D < r_n$, the $\{\mathbf{y}_i\}$ are at least r_n apart and one obtains a better packing fraction using the same set of $\{\mathbf{y}_i\}$ with $D = r_n$.

There are two natural ways to specify which spheres are neighboring in a packing. One says two spheres (disks) have a *hard contact* if $|\mathbf{y}_i - \mathbf{y}_j| = (D_i + D_j)/2$. This is a kind of bond; however the term "bond" will be reserved for bonds defined by the Voronoi criterion, which is a more useful one. In the Voronoi construction, given an arbitrary set of distinct points $\{\mathbf{y}_i\}$ we associate to each \mathbf{y}_i

a domain, the Voronoi cell, of all points nearer to it than to any other y_i . Points are called *neighbors*, connected by a *bond*, if their cells share a face (edge in two dimensions). The number of bonds to a point is its *coordination number* Z .

For $\{y_i\}$ chosen from Penrose tiling vertices, the set of possible nearest-neighbor locations is discrete. Then there will be a nonzero density of situations—four points in a rectangle or trapezoid—where the Voronoi construction becomes singular; here I choose to say that *neither* diagonal pair has a bond. Typically, the Voronoi bond network of a 3D packing forms the edges of a set of tetrahedra (and, in places where the construction became singular, octahedra) which fill space; in the case of a 2D packing, space is filled by triangles (and rectangles, trapezoids, pentagons, ...).

C. Outline

An outline of the rest of the paper is as follows. Section II considers the two-dimensional Penrose tiling (2D PT), showing how a sphere packing may be constructed on it, and how this packing relates to various structures described by previous authors. The 2D PT is discussed mainly to illustrate concepts which are applied to the (more complicated) 3D PT in later sections; in its actual content, Sec. II is independent of the rest. Section III introduces the 3D Penrose tiling: first the “projection” method of its construction is outlined, and then this is applied in a detailed investigation of the statistics of local environments. With this information, it is then possible to construct a good sphere packing.

In Sec. IV, the same treatment is applied to the “twelve-fold” vertices, an interesting subset of 3D PT sites. Section V discusses how the density maxima in the density-wave models can be interpreted as packed spheres, and how the latter can be interpreted as clusters of atoms in a model of the $i(\text{Al-Mn})$ structure.^{8,9} Section VI concludes. Three Appendices contain proofs and useful techniques based on the projection construction.

II. TWO-DIMENSIONAL PENROSE TILING

A. Vertices and local environments in two dimensions

The motivation for studying the two-dimensional Penrose tiling (2D PT) is in part didactic: It is easier to construct, depict, and visualize than the 3D PT. The 2D PT has already been used in various atomic models.^{12,25-29} Furthermore, it seems to describe the rapidly quenched phase $T(\text{Al-Mn})$,^{30,31} and is closely related to the Al_3Fe structure.^{10,14}

The properties of the two-dimensional Penrose tiling have been reviewed elsewhere.^{25,32-34} It is a packing of two kinds of rhombus with edge a : a large kind (L), with acute angle $2\pi/5$, and a small kind (S) with acute angle $\pi/5$ (see Fig. 1). They have areas

$$A_L = a^2 \sin(2\pi/5) = a^2 [(5 + \sqrt{5})/8]^{1/2} \tag{1a}$$

and

$$A_S = a^2 \sin(\pi/5) = \tau^{-1} A_L \tag{1b}$$

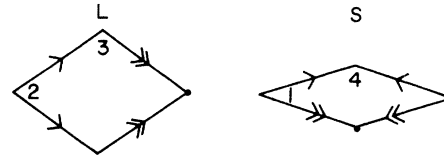


FIG. 1. Large (L) and small (S) Penrose rhombi; arrows represent the matching rules. The corner angles are indicated in units of $\pi/5$. The heavy dots mark the “pole” vertices (see text).

The arrow markings on adjoining edges are required to match. [There is another representation^{32,33(a)} in terms of objects known as “kites” (K) and darts (D).] Vertices where double arrows converge are called “poles” by Mackay.²⁵

The most efficient way to generate the 2D PT is by “deflation,”^{25,26,29,32-34} a process in which rhombi are replaced by geometrically similar ones with edge length smaller by a factor of the golden ratio $\tau \equiv (1 + \sqrt{5})/2$. (The 2D PT can also be generated by “projection” from a high-dimensional space as outlined in Appendix A.) Deflation has been illustrated already in Refs. 25, 32, and 33(a); here (see Fig. 2) I show how one can perform *half* deflations to go from an (L, S) tiling to a (K, D) tiling to a deflated (L', S') tiling.

Let us represent a rhombus corner with interior angle

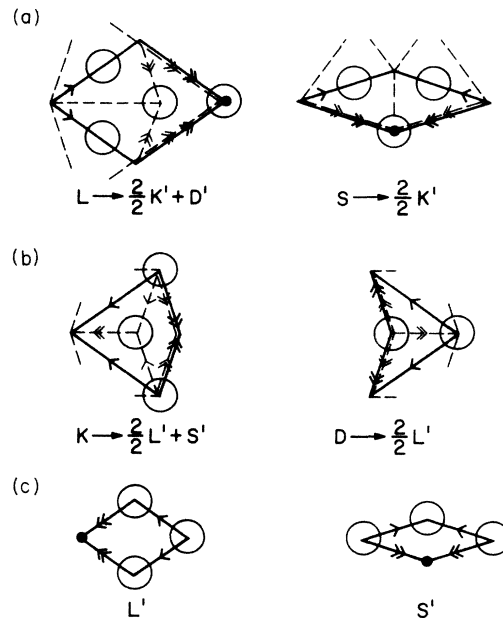


FIG. 2. Deflation of the Penrose tiling in two stages: (a) from rhombi to kites and darts; (b) from kites (K) and darts (D) to deflated rhombi; (c) deflated rhombi. In (a) and (b) the dashed lines and light arrows refer to the “deflated” objects. In (a) and (c), the “poles” at these respective scales are marked by dots. The circles in (c) mark the nonpole sites, where disks are packed in disk packing (i) of the Sec. II B; these same circles are marked in (a) and (b) to show how the *same* packing appears on larger tiles. Note that in (a) and (b) the circles would suffice to force the matching rules, but this is not the case in (c).

$k\pi/5$ by $\langle k \rangle$, or by $\langle k \rangle^*$ if the corner is at a "pole." We see there are only six types of corner: In the L , $\langle 2 \rangle$, $\langle 2 \rangle^*$, and $\langle 3 \rangle$; in the S , $\langle 1 \rangle$, $\langle 4 \rangle$, and $\langle 4 \rangle^*$ (see Fig. 1). The whole vertex is represented by $\langle k_1 k_2 \dots \rangle$; here obviously $\sum_i k_i = 10$. In the deflation, each of the single-arrowed edges generates a $\langle 433 \rangle$ vertex, or (since each rhombus has two such edges)

$$L, S \rightarrow \frac{1}{2} \langle 433 \rangle . \tag{2a}$$

Also, an interior vertex is generated:

$$L \rightarrow \langle 33121 \rangle . \tag{2b}$$

Inspection of Fig. 2 shows that the corners map as follows when rhombi are deflated:

$$\begin{aligned} \langle 1 \rangle &\rightarrow \frac{1}{2} \langle 2 \rangle^* , \\ \langle 2 \rangle &\rightarrow \langle 2 \rangle^* , \\ \langle 2 \rangle^* &\rightarrow \frac{1}{2} \langle 2 \rangle + \frac{1}{2} \langle 2 \rangle , \\ \langle 3 \rangle &\rightarrow \frac{1}{2} \langle 2 \rangle^* + \frac{1}{2} \langle 4 \rangle^* , \\ \langle 4 \rangle &\rightarrow \frac{1}{2} \langle 4 \rangle^* + \frac{1}{2} \langle 4 \rangle^* , \\ \langle 4 \rangle^* &\rightarrow \frac{1}{2} \langle 2 \rangle + \langle 1 \rangle + \langle 1 \rangle + \frac{1}{2} \langle 2 \rangle . \end{aligned}$$

From this we can derive

$$\langle 433 \rangle \rightarrow \langle 422 \rangle^* \rightarrow \langle 2211211 \rangle \rightarrow \langle 22222 \rangle^* , \tag{3a}$$

$$\langle 33121 \rangle \rightarrow \langle 4222 \rangle^* \rightarrow \langle 222211 \rangle \rightarrow \langle 22222 \rangle^* , \tag{3b}$$

and also

$$\langle 22222 \rangle^* \leftrightarrow \langle 22222 \rangle . \tag{3c}$$

Thus, there are only eight types of vertex³² (Fig. 3), of which three (with asterisks) are "pole" vertices. Around each vertex in the bottom row, one can pick out neighbors which form a perfect pentagon; I will call these "fivefold vertices" (they are called "suns" in Ref. 32). These form the τ^2 inflation of the 2D PT. The sites $\langle 22222 \rangle$ and $\langle 22222 \rangle^*$ have no neighbors besides the pentagon so they have fivefold symmetry; I will call them "perfect fivefold sites." (In the 3D PT case, the analogous subsets—"twelfold" and "perfect twelfold" vertices—also form interesting superstructures; see Sec. IV.)

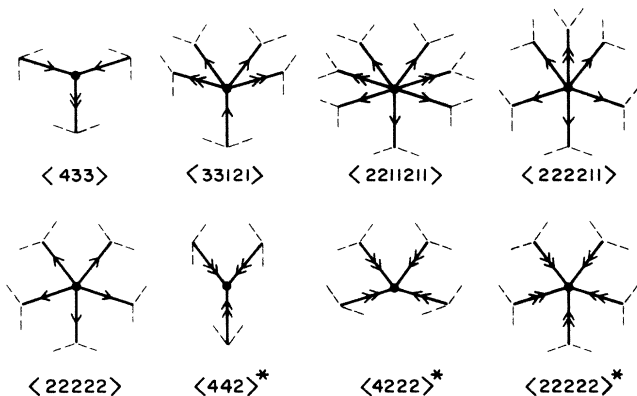


FIG. 3. The eight allowed vertex types in the 2D PT.

TABLE I. Vertices in the 2D PT.

Vertex	Name ^a	$\alpha \beta \gamma$	Frequency
$\langle 433 \rangle$	<i>D</i>	3 2 1	τ^{-2} (0.3820)
$\langle 33121 \rangle$	<i>J</i>	5 2 0	τ^{-3} (0.2361)
$\langle 442 \rangle^*$	<i>Q</i>	3 0 2	τ^{-4} (0.1459)
$\langle 4222 \rangle^*$	<i>K</i>	4 0 1	τ^{-5} (0.0902)
$\langle 2211211 \rangle$	<i>S3</i>	7 0 0	τ^{-6} (0.0557)
$\langle 222211 \rangle$	<i>S4</i>	6 0 0	τ^{-7} (0.0344)
$\langle 22222 \rangle^*$	<i>S</i>	5 0 0	$\tau^{-5}/\sqrt{5}$ (0.0403)
$\langle 22222 \rangle$	<i>S5</i>	5 0 0	$\tau^{-7}/\sqrt{5}$ (0.0154)

^aAs used in Ref. 32.

A striking feature of the 2D PT is the self-similarity of the spatial distribution of different kinds of vertices. In particular, consider the pattern made by taking all the "nonpole" vertices. (This is just variation 2 of the "unit disk packing;" see below.) The following subsets of sites form inflations of this pattern by factors of τ , τ^2 , τ^3 , and τ^4 , respectively: (i) all "pole" vertices; (ii) all $\langle 22222 \rangle$, $\langle 2112112 \rangle$, and $\langle 221122 \rangle$ vertices (i.e., all nonpole "fivefold" vertices); (iii) all $\langle 22222 \rangle^*$ vertices; (iv) all $\langle 22222 \rangle$ vertices.

We can easily derive the frequencies of the different vertices. [See also Ref. 33(b); a more rigorous treatment of the frequencies of arbitrary patterns in the 2D PT is given in Ref. 34.] I will normalize all frequencies of local environments by the density of vertices, which is the same as the (number) density of rhombi:³⁵ $n(L) + n(S) = 1$. Thus, since

$$n(L)/n(S) = \tau , \tag{4}$$

(which follows easily^{25,32} from the deflation rule) we have $n(L) = \tau^{-1}$ and so, for example, using (2a) the frequency of vertex $\langle 433 \rangle$ is

$$n(\langle 433 \rangle) = \tau^{-2} n(L) = \tau^{-3} .$$

(The factor τ^{-2} comes because there are τ^2 new vertices for each old vertex.) Continuing this way, we derive the results in Table I (the frequencies add up to 1, of course).

A different way we can classify the vertices is to perform a Voronoi construction (see Fig. 7 of Ref. 26). In fact, if we decorate each rhombus as shown in Fig. 4, then the dashed lines will make up the Voronoi cell edges. Thus, there are three kinds of neighbor bonds: those at distance a , which are connected by Penrose tiling edges;

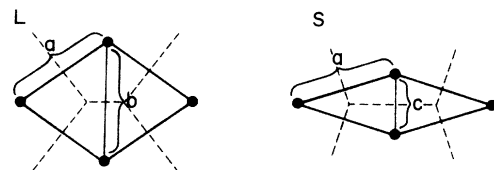


FIG. 4. Penrose rhombi showing Voronoi cell edges (dashed lines). The nearest-neighbor bonds a , b , and c are shown (solid lines). These divide the plane into triangles, with every vertex having 5, 6, or 7 neighbors.

short bonds across an S rhombus [Fig. 4(b)] at distance $c \equiv 2a \sin(\pi/10) = \tau^{-1}a \cong 0.618a$; and “long” bonds across an L rhombus, at distance

$$b \equiv 2a \sin(\pi/5) = [(5 - \sqrt{5})/2]^{1/2}a \cong 1.176a .$$

For every $\langle 3 \rangle$ corner at a vertex, we have one b neighbor; for every $\langle 4 \rangle$ corner we have a c neighbor. Of course, the total number of corners is the number of a neighbors. Defining α , β , and respectively, γ as the number of a , b , and c neighbors, we get the numbers shown in column 3 of Table I. It is easy to check (Fig. 4) that the a , b , and c bonds correspond one-to-one with rhombus edges, L 's, and S 's, respectively, and so the averages are $\bar{\alpha} = 4$, $\bar{\beta} = 2\tau^{-1}$, and $\bar{\gamma} = 2\tau^{-2}$. For the total coordination number $Z = \alpha + \beta + \gamma$ we have $Z = 5$ (from the three “pole” vertices and $\langle 2222 \rangle$), $Z = 6$ (from $\langle 433 \rangle$ and $\langle 222211 \rangle$), or $Z = 7$ (from $\langle 33121 \rangle$ and $\langle 2211211 \rangle$), with frequencies $n(Z=5) = n(Z=7) = 2\tau^{-4} \cong 0.292$; thus $\bar{Z} = 6$, as must be true in two dimensions (by Euler's theorem).

B. Packings on the 2D PT

The a and b distances are similar in magnitude and can accommodate disks of diameter $D = a = 1$. The “short” c bonds do not allow this, but there are relatively few of them, so we can make a reasonable packing of unit disks by removing a disk at one end of each short bond.

1. Unit disk packing

In the densest possible packing of this type by identical disks, the only types of vertices which need be vacant are those with $\langle 4 \rangle^*$ corners, namely $\langle 422 \rangle^*$ and $\langle 222 \rangle^*$, which have a combined frequency of $\tau^{-3} \cong 0.236$ (so the occupied fraction is $1 - \tau^{-3} = 2\tau^{-2} \cong 0.764$). This is sufficient since one end of every c bond is a $\langle 4 \rangle^*$ corner. The average area per site is

$$\bar{A} \equiv \tau^{-1}A_L + \tau^{-2}A_S = \frac{5}{2}\tau^{-2}(\tau/\sqrt{5})^{1/2} \cong 0.8117a^2$$

so the packing fraction is

$$f = (\pi a^2/4)(2\tau^{-2})/\bar{A} \cong (0.5950)/(0.8117) \cong 0.738 . \quad (5)$$

This packing is illustrated in Fig. 5.

For comparison, a triangular lattice (close packing) has $f = \pi/2\sqrt{3} \cong 0.907$, a square lattice has $f = \pi/4 \cong 0.785$,

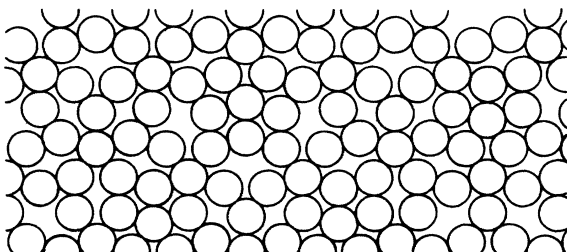


FIG. 5. Unit disk packing on the 2D PT (compare Fig. 4 of Ref. 25, from which this is adapted).

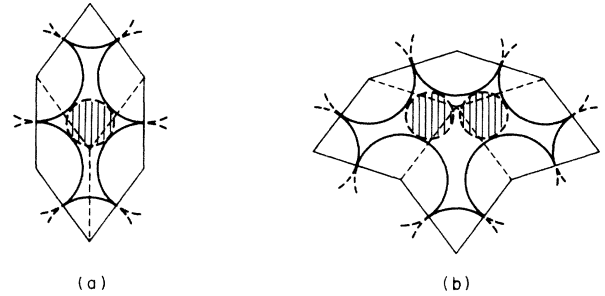


FIG. 6. Holes arising from the unused vertices (at junction of dashed rhombus edges) in the packing by disks of unit diameter. In the absence of the hatched disks, the two open disks (at bottom) are free to move up into the hole and the packing is not rigid. The holes may be filled by adding disks (hatched) of diameter $D' \cong 0.54$.

and a honeycomb lattice has $f = \pi/3\sqrt{3} \cong 0.605$. Also, the 2D “random close packing”^{36,37} has $f_{\text{RCP}} \cong 0.82$. Thus, the unit disk packing is rather loose. On the other hand, its 3D analog (see Sec. III C) has a packing fraction close to random close packing.

One would like to check whether the packing is actually mechanically stable: i.e., are interior motions impossible, if one fixes all disks on the surface of a finite cluster. A weaker criterion (its advantage is being easy to check) is *local* stability: does every semicircle around every disk include at least one neighbor (in this case an a neighbor) in hard contact? Unfortunately, the unit disk packing is *not* locally stable since the neighbors along the edges between $\langle 2 \rangle$ corners next to the vacant $\langle 422 \rangle^*$ site are loose [see Fig. 6(b)].

2. Unit disk packing: Second variation

We have removed disks from two of the “pole” sites; if we also remove them from $\langle 2222 \rangle^*$, i.e., from *all* of the “pole” sites, we get the disk packing shown by Mackay²⁵ in his Fig. 4. A fraction $(6\tau^{-5} + \tau^{-6})/\sqrt{5} \cong 0.2664$ of all sites are vacant. The same packing describes one of the layers of an idealized Al_3Fe structure, with an Fe atom occupying the $\langle 2222 \rangle$ site and Al atoms in the other ones.^{10,14} It also describes the pattern of bright spots in high-resolution electron images of the icosahedral $(\text{Ti}_{0.9}\text{V}_{0.1})_2\text{Ni}$ phase.³⁸

It is, in fact, very natural to find this pattern in layered structures which are stackings of decorated Penrose tilings. The reason is that any 2D PT can also be interpreted as a puckered surface in 3-space, called a “Wieringa roof,”³² which we are looking down on; the L and S rhombi are imagined to be identical, but tipped so they are foreshortened in different ways. It turns out that there are only four possible values for the altitude coordinate, and the outer two values correspond to the “poles” so their removal leaves a much flatter layer.

3. Unit disk packing: Third variation

In the unit disk packing all $\langle 2222 \rangle$ disks—and also (since we removed $\langle 442 \rangle^*$ sites) all $\langle 2211211 \rangle$ and

$\langle 22211 \rangle$ disks—have the same (pentagonal) surroundings as the $\langle 2222 \rangle^*$ disks which were removed in the first variation. If we vacate *all* of these “fivefold” sites, we get the decoration shown by Mosseri and Sadoc in Fig. 7 of Ref. 27, or Fig. 5 of Ref. 28. It contains only $\langle 433 \rangle$ and $\langle 33121 \rangle$ vertices. As they note, the remaining a and b bonds form a perfect fourfold-coordinated net.

They defined defects by comparing this network to an ideal structure which exists on a curved surface; the resulting defect arrays had a hierarchical, self-similar structure. In view of the self-similar distribution of environments in the 2D PT (noted at the end of Sec. II A), this result is hardly surprising.

4. Pentagon packing

It is amusing to note that we can achieve a better packing by replacing the spheres of variation of 2 by pentagons, as indicated in Fig. 7. (Compare this to the pentagon packings illustrated in Refs. 12, 26, and 38.) The packing fraction is $f = \tau/2 \cong 0.809$. A related pentagon packing has been used in a hypothetical model of (i) (Al-Mn).¹²

Recently a random packing of edge-sharing pentagons³⁹ was found to have a diffraction pattern similar to that of the 2D PT. The random packing has a local order similar to that of Fig. 7(b), but the packing fraction appears to be much lower.

For comparison, we should consider crystalline packings of the same pentagons. Four examples are shown in Fig. 8. Here Figs. 8(a) and 8(c) show packings where the pentagon centers form a triangular lattice with a rectangular distortion: $b/a = \sqrt{3}$ becomes ~ 1.539 in 8(a) and ~ 1.577 in 8(c). The packing fractions are, respectively, $\sqrt{5}\tau^2 \cong 0.854$ in 8(a) and $2\sqrt{5}/3\tau \cong 0.921$ in 8(c). The packing in 8(c) seems to be the closest packing of pentagons in two dimensions. Indeed, in a gas of hard pentagons which was slowly frozen,²⁴ we find a large single domain of the Fig. 8(c) packing (upper half of Fig. 3 in Ref. 24); however, packing like Fig. 8(b) is favored in the two or three layers next to the walls, and packing like Fig. 8(a) occurs in some regions (possibly grain boundaries).

The pentagon packings of Figs. 8(a) and 8(c) differ from the quasicrystal packing [Fig. 7(b)] in having fewer

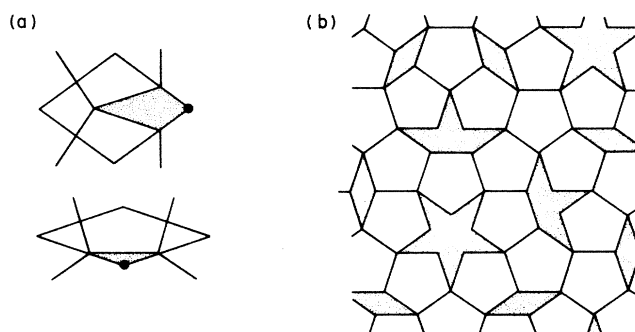


FIG. 7. Pentagon packing on the 2D PT. Decorating Penrose rhombohedra as in (a) (the dots indicate the “pole” vertices here) generates the packing shown in (b).

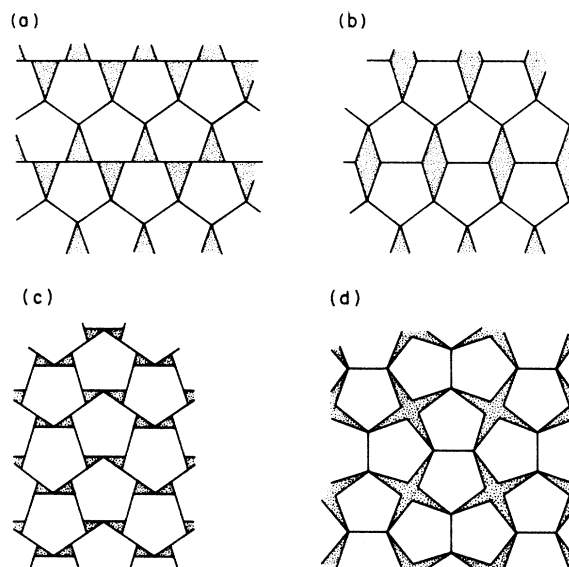


FIG. 8. Crystalline packings of pentagons. Packing fractions: (a) and (b), 0.854; (c), 0.921; (d) 0.828.

shared edges. If we try to maximize the number of shared edges, it appears the optimal packing is that of Fig. 8(b), which has the same packing fraction as Fig. 8(a) but is obviously closer to Fig. 7(b) in its local order. It can be generated by making elongated hexagonal cells of one L and two S rhombi [like Fig. 6(a)], packing them on the plane, and decorating them as in Fig. 7(a). The 8(b) structure gives an alternate description of the layered phase Al_3Fe .¹⁴ (The pentagons represent clusters in the form of bipentagonal pyramids with composition $\text{Al}_{16}\text{Fe}_7$).

The periodic packings are also found in packings of tubes composed of stacks of pentagonal capsomeres (virus fragments).⁴⁰ Figures 3(a) and 3(b) of Ref. 40, are, respectively, similar to Fig. 8(a) and identical to Fig. 8(b).

5. Packings with two sizes of disk

If another size of disk is allowed, the unit disk packing can be improved. We can place disks of diameter $D' = (a^2 + b^2)^{1/2} - a \cong 0.543$ in the gaps around vacant vertices—one disk in the $\langle 244 \rangle^*$ gap and two in the $\langle 4222 \rangle^*$ gap (see Fig. 6). There are $\tau^{-4}\sqrt{5} \cong 0.326$ small disks per vertex, i.e., the number ratio is $n(D')/n(D) = \tau^{-2}\sqrt{5}/2$, and the packing fraction is $f \cong 0.832$. This can be compared to regular lattices with small disks filling interstitial holes: (a) square lattice, $D'/D = (\sqrt{2} - 1) \cong 0.414$, $n(D')/n(D) = 1$, and $f \cong 0.926$; (b) honeycomb lattice (with three small disks in each hole), $D'/D \cong 0.516$, $n(D')/n(D) = 1$, and $f \cong 0.847$.

Another interesting disk packing on the 2D PT has been discovered by Socolar and Steinhardt (see Ref. 29, Fig. 6). They place a disk of radius $D = \tau^{-1}$ on every vertex of the 2D PT; in addition one is placed in the interior of every L rhombus *away* from the “pole” end, dividing the long diagonal in the ratio $\tau^{-1}:\tau^{-2}$. (The interior site is not a vertex of *any* deflation of τ of the 2D PT so it does *not*

belong to the class of packing I consider elsewhere in this paper.) Smaller disks of diameter $D' \cong 0.575$, $D \cong 0.355$ are placed, two per rhombus (both L and S), to fill the interstices; the packing fraction is $f \cong 0.842$.

III. SPHERES ON (MOST) VERTICES OF 3D PENROSE TILINGS

A. Projection method for constructing 3D PT

We shall follow the same path for the three-dimensional Penrose tiling (3D PT) as for the two-dimensional one. However, the 3D PT is most naturally constructed by projection from a six-dimensional (6D) simple cubic lattice^{3,6,41,42} rather than by deflation rules (which become complicated^{29,43} in 3D). I will describe the method briefly, focusing on its application rather than its justification.

We let $\{\hat{e}_1, \hat{e}_2, \dots, \hat{e}_6\}$ be a set of unit vectors in three-dimensional “physical” space in icosahedral directions (i.e., $\{\pm \hat{e}_i\}$ form the vertices of a regular icosahedron). To each \hat{e}_i we associate a corresponding vector \hat{e}_i^\perp , in another three-dimensional “pseudospace”⁴ orthogonal to the physical space. The $\{\hat{e}_i^\perp\}$ also form an icosahedral set, but permuted so that

$$\hat{e}_i \cdot \hat{e}_j = \pm 1/\sqrt{5} \implies \hat{e}_i^\perp \cdot \hat{e}_j^\perp = -\hat{e}_i \cdot \hat{e}_j \quad \text{for } i, j = 1, 2, \dots, 6. \quad (6)$$

In other words, if \hat{e}_i and \hat{e}_j are nearest neighbors on the icosahedron, then \hat{e}_i^\perp and \hat{e}_j^\perp are second neighbors, and vice versa.

The physical quasilattice vertices are of the form

$$\mathbf{x}_{[n]} = \mathbf{x}_0 + \sum_{i=1}^6 n_i \hat{e}_i, \quad (7)$$

where $[n] = [n_1, n_2, \dots, n_6]$ is a set of integers which are in fact the coordinates in the 6D lattice. Not every point

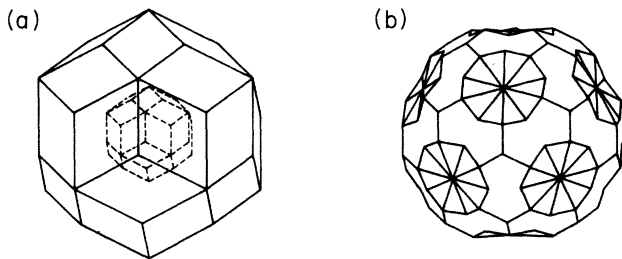


FIG. 9. (a) Rhombic triacontahedron \mathcal{C} , which is the “acceptance domain” in pseudospace that determines which points are included in the projection construction of the 3D PT. It has diameters 2.753, 2.384, and 3.236 along the twofold, threefold, and fivefold axes, respectively. The dashed triacontahedron, which is smaller by a factor τ^2 , is the sector \mathcal{C}_{12} corresponding to the “twelvefold” vertices. (b) Expanded view of the smaller triacontahedron \mathcal{C}_{12} , after caps have been removed to make a sector \mathcal{S}_{12} representing the $D=2.38$ (“twelvefold”) sphere packing. The respective diameters are 1.051, 0.905, and 1.000 (1.236 in the fivefold direction before the caps were removed).

of form (7) appears in the 3D PT; we associate with each $\mathbf{x}_{[n]}$ a pseudospace point

$$\mathbf{x}_{[n]}^\perp = \mathbf{x}_0^\perp + \sum_{i=1}^6 n_i \hat{e}_i^\perp \quad (8)$$

and include $\mathbf{x}_{[n]}$ in the 3D PT if and only if $\mathbf{x}_{[n]}^\perp$ lies within a domain \mathcal{S} , which will be called the *acceptance domain*. Here we take the acceptance domain to be

$$\mathcal{C} \equiv \left\{ \mathbf{x}_0^\perp + \sum_{i=1}^6 \xi_i \hat{e}_i^\perp : 0 \leq \xi_i \leq 1 \right\}, \quad (9)$$

i.e., the 3D projection of the hypercubic unit cell of the 6D lattice of $[n]$'s. In fact, \mathcal{C} is a rhombic triacontahedron [Fig. 9(a)] with unit edges oriented in icosahedral directions. For later use, I also note that if we took \mathcal{S} to be a strict subset of \mathcal{C} , then $\{\mathbf{x}_{[n]}\}$ would form a subset of the 3D PT vertices. No matter what \mathcal{S} we use, the resulting structure has a diffraction pattern with the same spot positions as for the 3D PT proper.

This construction gives a packing of 3-space by two kinds of rhombohedral cell, with edges of unit length in icosahedral directions (Fig. 10), which I will call P (“prolate”) and O (“oblate”). Their faces are identical rhombi with acute angle $\cos^{-1}(1/\sqrt{5}) \cong 63.4^\circ$; their volumes are

$$V_P = \frac{4}{3} a^3 [(5 + \sqrt{5})/8]^{1/2}, \quad V_O = \tau^{-1} V_P \quad (10)$$

and their numbers are in the ratio^{26,44}

$$n_P/n_O = \tau. \quad (11)$$

The average volume per site is

$$\begin{aligned} \bar{V} &\equiv \tau^{-1} V_P + \tau^{-2} V_O \\ &= 2a^3 (1 - 2/\sqrt{5})^{1/2} \cong 0.6498. \end{aligned} \quad (12)$$

B. Local environments and neighbors

To determine the local environment around a vertex \mathbf{x} of the 3D PT, it suffices to know the location of \mathbf{x}^\perp within \mathcal{C} . For example, \mathbf{x} has a neighbor at $\mathbf{x}_{[n]} + \hat{e}_1$ if and only if $\mathbf{x}_{[n]}^\perp + \hat{e}_1^\perp \in \mathcal{C}$, i.e., $\mathbf{x}_{[n]}^\perp$ is within the subdomain (“sector”) $\mathcal{C} \cap (\mathcal{C} - \hat{e}_1^\perp)$. [Here “ $(\mathcal{C} - \hat{e}_1^\perp)$ ” denotes the domain \mathcal{C} , translated by $-\hat{e}_1^\perp$.] One can construct successively more refined sectors representing the specification of the positions of neighbors out to succes-

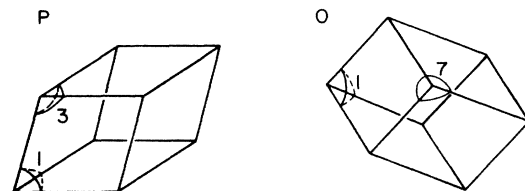


FIG. 10. The prolate (P) and oblate (O) rhombohedra, showing the corner spherical angles in multiples of $\pi/5$.

TABLE II. Vertex separations in 3D PT.

Name	r	r^2	Vector	Frequency
c	0.563	$3-6/\sqrt{5}$	[111000]	$0.76 (2\tau^{-2})^a$
a	1.000	1	[100000]	6^a
b	1.052	$2-2/\sqrt{5}$	[1 $\bar{1}$ 0000]	$6.5 (6+2\tau^{-2})^a$
d_1	$1.451=(a^2+b^2)^{1/2}$	$3-2/\sqrt{5}$	[11 $\bar{1}$ 000]	7.7
d_2	$1.487=\sqrt{2}b$	$4-4/\sqrt{5}$	[11 $\bar{1}$ 100]	2.2
b'	$1.701=\tau b$	$2+2/\sqrt{5}$	[110000]	14.2
d_3	1.792	$5-4/\sqrt{5}$	[2 $\bar{1}$ 0000]	0.82
e_1	1.973	$3+2/\sqrt{5}$	[110100]	18.4
a_1	2.000	4	[200000]	1.42
d_4	2.000	4	[11 $\bar{1}$ 010]	7.5
a_2	2.236	5	[011111]	0.76
d_5	2.236	5	[01111 $\bar{1}$]	4.2
f_1	2.260	$6-2/\sqrt{5}$	[21 $\bar{1}$ 000]	1.09
c'	$2.384=\tau^3 c$	$3+6/\sqrt{5}$	[111000]	14.1
d'_2	$2.406=\tau d_2$	$4+4/\sqrt{5}$	[111 $\bar{1}$ 00]	17.4
d_6	2.471	$7-2/\sqrt{5}$	[21 $\bar{1}$ 100]	0.26
e_2	2.606	$5+4/\sqrt{5}$	[210000]	11.3
f_2	2.626	$6+2/\sqrt{5}$	[2 $\bar{1}$ 0100]	7.7
b''	$2.753=\tau^2 b$	$4+8/\sqrt{5}$	[111100]	19.9
f_3	2.810	$7+2/\sqrt{5}$	[211 $\bar{1}$ 00]	3.3
d_7	2.929	$5+8/\sqrt{5}$	[111110]	24.7
c_1	$2.947=2\tau^2 c$	$6+6/\sqrt{5}$	[1111 $\bar{1}$ 1]	3.6
e_3	2.947	$6+6/\sqrt{5}$	[210100]	10.2
a_3	3	9	[300000]	0.01

^aExact value [see Eqs. (14)].

sively larger radii in physical space.⁴² The pseudospace vertices $\{\mathbf{x}_i^\dagger\}$ are distributed uniformly over \mathcal{C} ; consequently, the frequency of any given environment in the 3D PT is proportional to the volume fraction of \mathcal{C} occupied by the corresponding sector.⁴²

As an example of an environment, consider the “twelvefold” vertices,⁴⁵ defined by the presence of all twelve possible rhombohedron edges around them (this subset is the basis of Sec. IV, below). Their sector, which I will call \mathcal{C}_{12} , turns out to be a triacontahedron⁴² smaller than \mathcal{C} by a factor τ^{-2} [see Fig. 9(a)]; hence the frequency of twelvefold vertices is τ^{-6} .

The neighbor separations⁴² which occur in the 3D PT are listed in Table II, up to $r=3a$. Their frequencies were found numerically by counting the separations from vertices corresponding to $N=200\,000$ random points in \mathcal{C} . The separations named with a are in fivefold symmetry directions, those named with b are in twofold directions, those named with c are in threefold directions, those named with d and e are in mirror planes, and those named with f are in general directions. The frequencies are *sums* over all symmetry-equivalent separations (the respective degeneracies are a , 12; b , 30; c , 20; d and e , 60; f , 120). The lattice vector $[n_1, n_2, \dots, n_6]$ is given using the convention of Refs. 5, 7, and 42 for the directions of the $\{\hat{\mathbf{e}}_i\}$ (note that permutations and changes of sign of the n_i 's do *not* generally give an equivalent vector).

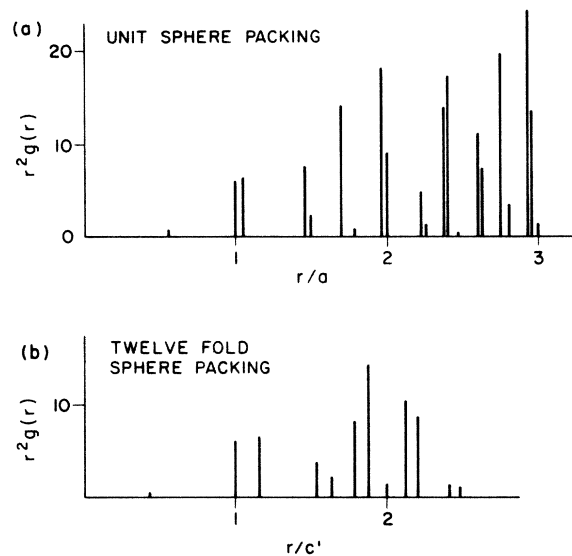


FIG. 11. Radial distribution function $r^2g(r)$ among (a) all 3D PT vertices (b) “superlattice” of “twelvefold” vertices. Every peak is a δ function; the vertical scale is its total weight (last columns of Tables II and VI). The radius r has been normalized by the diameters (a) $D=a$, and (b) $D=c'\cong 2.38a$, used in the corresponding sphere packings. In (b), the distribution function is shown only out to $r'/c'\cong 2.5$.

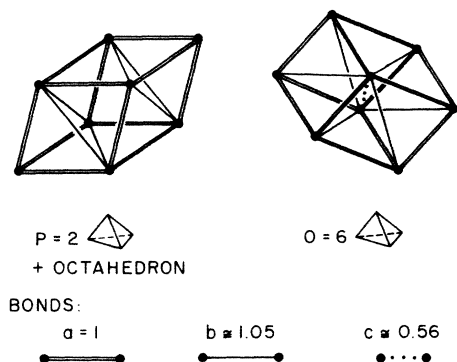


FIG. 12. Placement of Voronoi bonds on the prolate (P) and the oblate (O) rhombohedra, which are the "tiles" of the 3D PT.

The 3D PT radial distribution function (powder averaged over angles) is a sum of δ functions centered at the allowed separations; it is shown in Fig. 11(a). Note the striking resemblance to radial distribution functions arising from random close packings of hard spheres.^{19,20,24} The first four prominent rings consist of nearest neighbors at $r \cong a$, second neighbors across an approximate square (e.g., in octahedra) at $r \cong 1.4a$, and ordinary second neighbors at $r \cong 1.7a$ and $r \cong 2.0a$. However, whereas in the random-close-packed structure each ring formed a rounded peak, now each ring forms a discrete pair of peaks with a small splitting between them.

If we perform the Voronoi construction, we find that neighbors are all at separations a , b , and c . In fact, every edge of the 3D PT is an a bond, every short diagonal of a face rhombus is a b bond, and every short axis of the O rhombohedron is a c bond. To show this, we divide up each rhombohedron in analogy to Fig. 4 for the 2D PT; the resulting "bonds" are shown in Fig. 12. We can be sure that we will get proper Voronoi cells when we fit the rhombohedra together, because all the cell boundaries intersect the rhombohedron faces at right angles.

In the resulting bond network, the O rhombohedron is "triangulated" into six irregular tetrahedra; the P rhombohedron divides into two almost regular tetrahedra, at the tips, and a slightly distorted octahedron (there is an ambiguity in the Voronoi construction due to the $a-b-a-b$ rectangles visible in Fig. 12). Thus, the octahedra occupy a volume fraction $(2\tau/3)\sqrt{5} \cong 0.482$ of the packing; there is one octahedron per $(3\sqrt{5}+1)/2 \cong 3.854$ tetrahedra.

Note that every a separation is a rhombohedron edge, and every c separation is the short axis of an O rhombohedron, but not all b separations are b bonds. Rather, some b separations are second neighbors by two c bonds; these will be called \bar{b} neighbors.

On the other hand, every rhombohedron edge is an a bond, every face has a b bond, and every short axis of an O rhombohedron is a c bond. Thus, fractionally counting bonds on the surface according to the angle the rhombohedron subtends around them, every rhombohedron has three a and three b bonds (and, if it is an O rhombohed-

ron, it has a c bond). Also, it is obvious that (analogous to the 2D case) the number density of rhombohedra is one per vertex, i.e.,

$$n_P = \tau^{-1}, \quad n_O = \tau^{-2}. \quad (13)$$

Then, defining α , β , and γ as the number of a , b , and c coordinations, it follows that their averages are

$$\bar{\alpha} = 6, \quad (14a)$$

$$\bar{\beta} = 6, \quad (14b)$$

$$\bar{\gamma} = 2\tau^{-2}. \quad (14c)$$

Thus the average coordination number is

$$\bar{Z} \cong \bar{\alpha} + \bar{\beta} + \bar{\gamma} = 12 + 2\tau^{-2} \cong 12.764. \quad (15)$$

Because of the many octahedra, (15) is smaller than the "ideal" coordination for a random network of tetrahedra^{23,47}

$$Z_{\text{ideal}} \cong 13.4. \quad (16)$$

C. Classes of vertices and their frequencies

In the 3D PT, just as in the 2D PT, there are two approaches to classifying a vertex by its immediate local environment: (i) by the number and arrangement of rhombohedron corners which pack around the vertex and (ii) by the number and arrangement of its (Voronoi) first-neighbor vertices. These approaches (i) and (ii) are

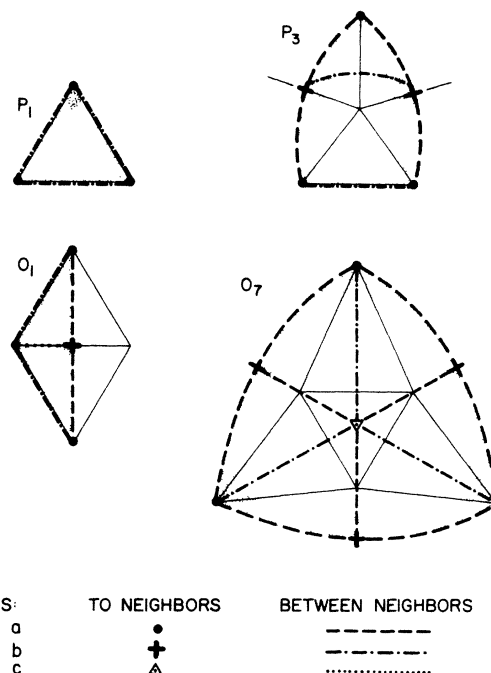
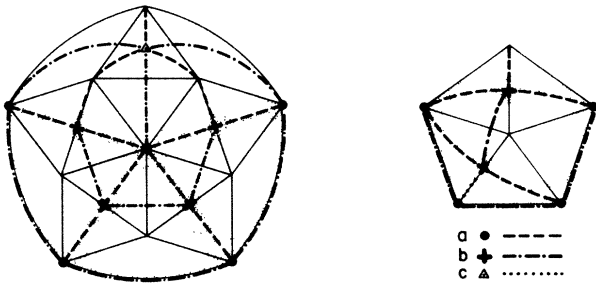


FIG. 13. The four kinds of corner spherical angle (compare Fig. 10) projected onto faces of an icosahedron around the corner vertex. Bonds to and among points in the nearest-neighbor coordination shell are indicated as explained in the key.



COORDINATION $(\alpha\beta\gamma) = (561)$
 CORNERS $4P_3 + O_1 + O_7$

FIG. 14. A frequent vertex in the 3D PT. The light solid "coordinate" lines are the edges of an icosahedron on which the local environment is projected (the cap from the bottom five faces is shown at the right). The vertices in the coordination shell and the Voronoi bonds between them are marked as in Fig. 13. The pattern of b neighbors arranged radially around the a bond at the center (of the left side of figure), is also found in most of the other kinds of vertex.

equivalent (see Appendix B 1).

Let us consider approach (i) first. There are just four kinds of rhombohedron corner, which I will label P_1 , P_3 , O_1 , and O_7 according to the rhombohedron type and the solid angle (in units of $\pi/5$). To represent how the solid angle around a vertex is apportioned into corners, it is

convenient to project it down onto the faces of a reference icosahedron (Figs. 13 and 14). Each face is a unit $\pi/5$ of solid angle.

One can also project the shell of nearest-neighbor vertices radially onto the same icosahedral "coordinates," as indicated by the point symbols in Fig. 14. Corners of a given type always have the same "decoration" of bonds extending into their solid angle (compare Figs. 12 and 13). As an example, one of the commonest 3D PT vertices is shown in Fig. 14.⁴⁸ Altogether, 24 distinct vertex types are allowed in the 3D PT (Ref. 41) (counting together those related by rotations and reflections of the icosahedral symmetry group). Diagrams like Fig. 14 have been drawn for each of them.⁴⁸ A common feature is the occurrence of rings of (up to five) b neighbors around a bonds.

The vertices are listed in Table III; they are labeled by $(\alpha\beta\gamma)_p$, where (α,β,γ) are the numbers of (a,b,c) neighbors as before, and p is the number of b neighbors in the most complete ring around an a bond (e.g., $p=4$ in Fig. 14). Note that $(\alpha\beta\gamma)$ uniquely specify the number of rhombohedron corners of each type which meet at a vertex (see Appendix B 2). For many combinations $(\alpha\beta\gamma)$, there is only one arrangement of rhombohedra around the vertex which actually occurs in the 3D PT (although many arrangements are geometrically possible). However, there are few "twelvefold" types where $(\alpha\beta\gamma)$ do not uniquely specify the environments; in these cases p is

TABLE III. Vertices in the 3D PT and their frequencies.

$(\alpha\beta\gamma)_p$	$N(P_1 P_3 O_1 O_7)$	s	$n^{(num)}$	n
$(452)_3$	0202	2-2	0.2358	τ^{-3} (0.2361)
$(561)_4$	1041	1	0.2354	τ^{-3} (0.2361)
$(661)_4$	1331	1	0.0553	τ^{-6} (0.0557)
$(670)_5$	0620	2	0.2369	τ^{-3} (0.2361)
$(770)_5$	1540	1	0.0558	τ^{-6} (0.0557)
$(870)_5$	2460	2	0.0684	$2\tau^{-7}$ (0.0689)
$(960)_4$	5360	1	0.0165	$2\tau^{-10}$ (0.0162)
$(970)_5$	3380	1	0.0263	$2\tau^{-9}$ (0.0263)
$(1050)_3$	8260	2-2	0.0031	τ^{-12} (0.0031)
$(1060)_4$	6280	1	0.0037	$2\tau^{-13}$ (0.0038)
$(1070)_5$	42100	2	0.0063	$2\tau^{-12}$ (0.0062)
$(1200)_0$	20000	$2^3 \cdot 3 \cdot 5$	0.01312	τ^{-9} (0.01316)
$(1210)_1$	18020	2-2	0.00316	τ^{-12} (0.00311)
$(1220)_2$	16040	2	0.00386	$2\tau^{-13}$ (0.00384)
$(1230)_p$	14060		0.00857	$2(\tau^{-12} + \tau^{-14})$ (0.00858)
$(1230)_2$		2-3		$2\tau^{-12}$ (0.00621)
$(1230)_3$		2		$2\tau^{-14}$ (0.00237)
$(1240)_p$	12080		0.00456	$2\tau^{-13} + \tau^{-15}$ (0.00457)
$(1240)_3$		1		$2\tau^{-13}$ (0.00384)
$(1240)_4$		2		τ^{-15} (0.00073)
$(1250)_p$	100100		0.01324	τ^{-9} (0.01316)
$(1250)_3$		2-2		$\tau^{-11} + \tau^{-13}$ (0.00694)
$(1250)_4$		2		τ^{-12} (0.00311)
$(1250)_5$		5		τ^{-12} (0.00311)
$(1260)_p$	80120		0.00544	$\tau^{-12} + 2\tau^{-14}$ (0.00548)
$(1260)_4$		1		$2\tau^{-14}$ (0.00237)
$(1260)_5$		2		τ^{-12} (0.00311)
$(1270)_5$	60140	2	0.00378	$2\tau^{-13}$ (0.00384)

necessary (and sufficient) to distinguish them.

For each vertex, Table III also lists s , the number of icosahedral symmetry operations which leave the local arrangement of corners and neighbors unchanged. This is factored to display the symmetry elements of that arrangement, e.g., $s=2\cdot3$ means a threefold axis and one kind of mirror plane, while $s=2^3\cdot3\cdot5=120$ means full icosahedral symmetry. Each vertex, then, has $120/s$ distinct orientations (if we counted these separately, we would find a total of 1693 different vertices).

The frequencies of the different vertices are evaluated by computing the volumes of the corresponding sectors of the triacontahedron \mathcal{C} in pseudospace. To do this exactly is a tedious exercise in elementary geometry. However, one notices that the resulting frequencies are always simple combinations of powers of τ^{-1} . Therefore, a “numerological” approach was used. First 250 000 random points were generated in \mathcal{C} and the frequencies $n^{(\text{num})}(\alpha\beta\gamma)$ were determined numerically. (To get adequate statistics for the last eight rows of Table III, an additional 100 000 random points were generated within \mathcal{C}_{12} , the sector of vertices with $\alpha=12$.) These frequencies^{49(a)} were then identified as integer multiples $n(\alpha\beta\gamma)$ (in a few cases, sums) of powers of τ^{-1} as shown in Table III. The proposed identifications satisfied $\sum n(\alpha\beta\gamma)=1$, and Eqs. (14).

The numerical method lumped together the vertices $(12\beta 0)_p$, which are distinguished only by p . To get their separate frequencies, the volume of every sector was calculated analytically, as described in Appendix B. All the identifications from the numerical results were confirmed; this supports use of the “numerological” method to find the frequencies of extended patterns which may be more difficult to handle analytically, such as the c chains of Table V (see below).

Roughly speaking, the sectors are nested with α increasing as one goes inwards from the (452) sectors at the surface of \mathcal{C} to be $(12\beta 0)$ sectors at its core. The $(12\beta 0)$ sectors are tiny silvers formed between intersecting planes which slice up the volume in a way closely analogous to the 2D case [Fig. 18(c)]. At the center is the sector of “perfect” (1200) sites, analogous to the dark shaded $\langle 2222 \rangle$ pentagon in Fig. 18(c). More details of the arrangement of sectors are given in Appendix B (see Table VIII).

For later use, let us turn our attention to the short c bonds. Since at most two of them come in to any vertex (note $\gamma \leq 2$ in Table III), they form chains. The longest

TABLE V. Frequencies $n_c(l)$ of chains of l short (c) bonds.

l	N_v	$n_c^{(\text{num})}$		n_c
1	1	0.05646	τ^{-6}	(0.05573)
2	1	0.05514	τ^{-6}	(0.05573)
4	2	0.02646	$2\tau^{-9}$	(0.02631)
5	3	0.00190	τ^{-13}	(0.00192)
8	4	0.00629	$2\tau^{-12}$	(0.00621)
10	5	0.00502	τ^{-11}	(0.00502)

such chain is a closed ring of 10 links in the form of a puckered decagon. Its center always lies on the midpoint of a 3D PT edge oriented along the decagon fivefold axis. The other c chains are fragments of this decagon with 1, 2, 4, 5, or 8 links. A \tilde{b} separation is just a second neighbor along such a chain. The sites with c bonds can be divided into subclasses labeled by $(\alpha\beta\gamma\tilde{\beta})$, where $\tilde{\beta}$ is the number of \tilde{b} separations. Their frequencies are shown in Table IV (derived from the same data^{49(a)} as in Table III).

The frequencies of c chains are also tallied, in Table V; the $n_c^{(\text{num})}$ were derived by generating 100 000 random points \mathbf{x}^1 in \mathcal{C} and following out the chain on which the corresponding vertex \mathbf{x} lies. This brute-force Monte Carlo numerical integration was again followed by numerology to get the n_c values. Note that the exact frequencies of the five possible combinations of $(\gamma\tilde{\beta})$ can be calculated from the inferred exact frequencies of Table V and independently from those of Table IV [e.g., $n(\gamma=1, \tilde{\beta}=0)=n(5610)+n(6610)=2n_c(1)$]. They can also be extracted using Table III and pictures of the local environments,⁴⁸ since every chain ($l > 2$) lies entirely in the neighbor shells of the two vertices on the chain’s axis; the results agree. Table V also lists $N_v(l)$, the number of vacant sites on a chain of l links in the “unit” sphere packing of the 3D PT, which is described next.

D. “Unit” sphere packing (based on 3D PT vertices)

Most of the Voronoi bonds between 3D PT vertices have length $a=1$ or $b \cong 1.05$; therefore, it is possible to make a reasonable packing with spheres of diameter $D=1$ on most of the vertices. This is exactly analogous to the “unit” disk packing on the 2D PT (Sec. II B): it suffices to ensure that one of the two endpoints of each c bond is left vacant. This is slightly harder to arrange on the 3D PT, since there is no essential asymmetry between the two endpoints of the c bond (compared to the 2D PT, where one endpoint is always a “pole” and the other is not). However, we can use the fact that the short bonds always form chains (or rings) to specify which sites are vacant: namely, every other site on the chain. For a chain of l links, the number of vacated sites is $N_v(l)=l/2$ when l is even and $N_v(l)=(l+1)/2$ when l is odd ($l=1$ or 5). It is clear that this is the optimal number, but it does not uniquely specify the placement. For the closed rings of 10 links, there are two ways to place the spheres (once we choose one site to be vacant, the rest are determined). For the even length chains, we must leave the endpoints occupied and this does determine the placement. For the odd

TABLE IV. Frequencies of $\tilde{\beta}$ values.

$\alpha\beta\gamma\tilde{\beta}$	$n^{(\text{num})}$		n
4520	0.0558	τ^{-6}	(0.0557)
4521	0.0680	$2\tau^{-7}$	(0.0689)
4522	0.1120	$2\tau^{-6}$	(0.1115)
5610	0.0681	$2\tau^{-7}$	(0.0689)
5611	0.1673	$3\tau^{-6}$	(0.1672)
6610	0.0423	$2\tau^{-8}$	(0.0426)
6611	0.0130	τ^{-9}	(0.0132)

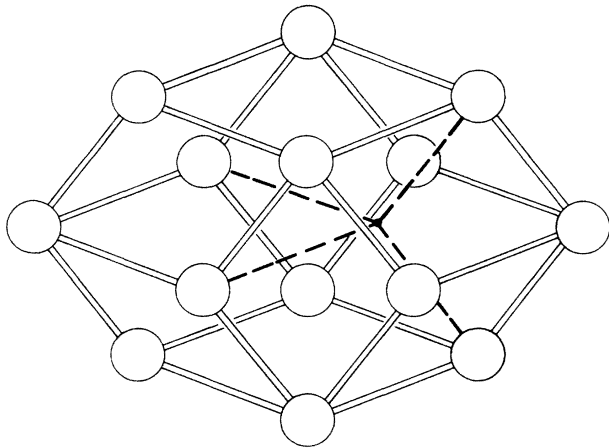


FIG. 15. A rhombic dodecahedron (RD), with occupied vertices indicated by spheres. The lines are 3D PT edges (dashed lines meet at the unoccupied site in the RD interior).

chains, there are $(l+3)/2$ ways to place the spheres so that adjacent neighbors on the c chain are never both occupied; however, if we also require that adjacent c neighbors are never both vacant, we have only two choices (determined by which endpoint site is vacant).

The unoccupied sites are all of type $(\alpha\beta\gamma)=(452)$, except for a few at endpoints of c chains. The sites surrounding a vacated (452) site form a “rhombic dodecahedron,” (RD) shown in Fig. 15 (the 3D analog of Fig. 6). In the even chains, the RD’s around the properly vacated sites almost always have twelfold sites at their tips.

Figure 15 suggests another way to view the procedure for vacating sites, in two stages. In the first stage, we group adjoining O rhombohedra (equivalently, connecting c links) into pairs. Between each pair the central (452) site is removed and the surrounding two O rhombohedra and two P rhombohedra are recombined into the RD, which becomes a new kind of tile in the structure. We create the maximum possible number of RD’s, but out of each odd chain one (isolated) O rhombohedron must remain. The second stage consists of removing an axis site from each remaining O rhombohedron (on a side where it is not touching an RD).

The advantage of the two-stage process is that its intermediate product—the tiling with RD tiles and a minimum of O tiles—is the basis for two decoration schemes describing real atomic structures.^{9–11} The number of RD’s per chain is $N_{RD}(l)=l/2$ (l even), $N_{RD}(l)=(l-1)/2$ (l odd), which gives a frequency of RD’s

$$n_{RD} = \sum_l n_l^{(c)} N_{RD}(l) = \tau^{-6} + 5\tau^{-8} \cong 0.1622. \quad (17)$$

Using Table V, the frequency of occupied sites is

$$\begin{aligned} n_{occ} &= 1 - \sum_l n_l^{(c)} N_v(l) \\ &= 1 - (6\tau^{-7} + \tau^{-9}) \cong 0.7802. \end{aligned}$$

The average volume per 3D PT site is \bar{V} given by (13), so

the packing fraction is

$$f = (\pi a^3/6) n_{occ} / \bar{V} \cong 0.6288. \quad (18)$$

This is essentially *identical* to the packing fraction of “random-close-packed” spheres,^{20,36}

$$f_{rep} \cong 0.64.$$

The unit sphere packing can be implemented as a projection with an acceptance domain \mathcal{S}_1 in place of (9). One first rephrases the conditions in the site-vacating rules in terms of local environment type, rather than c -chain length. [The diagrams of the environments⁴⁸ are essential to performing this translation, e.g., they tell us that the $l=8$ chains are the set of all chains with $(1070)_5$ and $(12\beta 0)_4$ sites on their axes.] Then the domain \mathcal{S}_1 is the (complicated) shape formed by subtracting from \mathcal{C} the sectors corresponding to vacated sites.⁵⁰

Although \mathcal{S}_1 is connected, it is far from being spherical (or even convex): Its diameters in the two, three, and fivefold directions are, respectively, 2.103 (reduced from S by a factor $2\tau^{-2}$), 2.384 (reduced by $\tau/2$), and 3.236 (not reduced at all). Note that \mathcal{S}_1 is a bit larger than the icosahedron which Ref. 6 chose as the acceptance domain.

IV. TWELVEFOLD VERTICES OF 3D PENROSE TILINGS

A. Distribution of twelfold sites

A different sphere packing, which (we shall see) seems related to the structure of the icosahedral Al-Mn-Si alloy,⁹ is based upon the subset of vertices which have all twelve possible edges radiating from them (“twelfold vertices”). As mentioned above, these correspond to an acceptance domain \mathcal{C}_{12} in pseudospace [Fig. 9(a)]; this is a triacontahedron like the 3D PT acceptance domain \mathcal{C} , but is reduced by a factor τ^2 so the twelfold sites have frequency τ^{-6} within the 3D PT.

The twelfold vertices do *not* form a twice “inflated” 3D PT, although they are distributed with the same density,^{49(b)} nor are they the vertices of any simply described tiling. Rather, the twelfold vertices form a sort of *approximate* superlattice, which I will call a “superstructure.”

There is a subset of the twelfold vertices, which I will call “perfect” twelfold vertices, with a perfectly icosahedral local environment. These sites have $(\alpha\beta\gamma)=(1200)$; at them, 20 sharp P_1 tips of the rhombohedral tiles meet. The “perfect” twelfold sites correspond in pseudospace to an acceptance domain which is yet another smaller triacontahedron, reduced from \mathcal{C} by a factor τ^3 ; thus the “perfect” 12’s are a fraction τ^{-3} of all twelfold sites. It turns out that⁵¹ the perfect 12’s are the τ^3 inflation of the 3D PT (see Fig. 16).

The allowed separations between twelfold sites up to $r=5a$ are listed in Table VI frequencies derived from 200 000 random points in \mathcal{C}_{12} . They are shown in Fig. 11(b). As in the unit sphere packing, one can identify double peaks corresponding to $r/D \cong 1.0, 1.4, 1.7,$ and 2.0 [if we take $D \cong 2.6a$, interpretable as a “soft-sphere” diameter, in place of the hard-sphere diameter $D \cong 2.38a$ used in Fig. 11(b)]. However, here the splitting of the

TABLE VI. Vertex separations in "superstructure" of twelfold sites.

Name	r	r^2	Vector	Frequency
a	1.000	1	[100000]	0.18 $(2\tau^{-5})^a$
c'	$2.384 = \tau^3 c$	$3 + 6/\sqrt{5}$	[111000]	5.9 $(6 - 2\tau^{-7})^a$
b''	$2.753 = \tau^2 b$	$4 + 8/\sqrt{5}$	[111100]	6.5 $(6 + 2\tau^{-3})^a$
(e)	3.642	$7 + 14/\sqrt{5}$	[211100]	3.9
d_2''	$3.893 = \sqrt{2}b''$	$8 + 16/\sqrt{5}$	[211101]	2.2
a'	$4.236 = \tau^3 a$	$9 + 20/\sqrt{5}$	[211111]	8.3
b'''	$4.453 = \tau^3 b$	$10 + 22/\sqrt{5}$	[212100]	14.2
(d)	5.052	$13 + 28/\sqrt{5}$	[222100]	10.6
a_5	5.236	$14 + 30/\sqrt{5}$	[311111]	1.41
d_4''	$5.236 = \tau^2 d_4$	$14 + 30/\sqrt{5}$	[22210]	7.4
(e)	5.753	$17 + 36/\sqrt{5}$	[32111]	1.40
(f)	5.916	$18 + 38/\sqrt{5}$	[320012]	1.09

^aExact value.

double peaks is much greater.

The closest allowed separations are $a=1$ (fivefold direction), $c' \cong 2.38$ (threefold direction), and $b'' \cong 2.75$ (twofold direction). These correspond roughly, but not necessarily precisely to the Voronoi neighbors within the twelfold superstructure (the b'' and c'' separations are also third-nearest neighbors within the 3D PT).

The number of separations to nearby twelfold sites of each type will be denoted α , γ' , and β'' .⁵² Sites will be la-

beled $(\alpha\beta''\gamma')_p$, where p is the number of b'' neighbors around a fivefold direction of the reference icosahedron, analogous to the p defined for the 3D PT. Table VII lists the frequencies of the different twelfold site types $(\alpha\beta''\gamma')$. There are 21 different environments (or 2010, if we distinguish orientations). As in the preceding section, the frequencies $n^{(\text{num})}$ were determined numerically from 1 000 000 random points in \mathcal{C}_{12} and then matched to polynomials in τ^{-1} . To get better statistics on the less fre-

TABLE VII. Vertex frequencies in the "superstructure" of twelfold points.

$(\alpha\beta''\gamma')_p$	s	$n^{(\text{num})}$		n
(175) ₅	2	0.1806	$2\tau^{-5}$	(0.1803)
(054) ₃	1	0.0162	$2\tau^{-10}$	(0.0163)
(055) ₃	1	0.0100	$2\tau^{-11}$	(0.0100)
(056) ₃	2·2	0.0289	$(\tau^{-8} + \tau^{-10})$	(0.0294)
(064) ₄	1	0.0956	$2(\tau^{-7} + \tau^{-9})$	(0.0952)
(065) ₄	1	0.0591	$2(\tau^{-8} + \tau^{-10})$	(0.0588)
(066) ₄	1	0.0263	$2\tau^{-9}$	(0.0263)
(076) ₅	1	0.1804	$2\tau^{-5}$	(0.1803)
(077) ₅ ^a	2	0.1668	$3\tau^{-6}$	(0.1672)
(007) ₀	2	0.01320	τ^{-9}	(0.01316)
(017) ₁	2	0.00312	τ^{-12}	(0.00311)
(027) ₂	1	0.00384	$2\tau^{-13}$	(0.00384)
(037) _p		0.00861	$2(\tau^{-12} + \tau^{-14})$	(0.00858)
(037) ₂	1		$2\tau^{-12}$	(0.00621)
(037) ₃	2		$2\tau^{-14}$	(0.00237)
(047) _p		0.00455	$2\tau^{-13} + \tau^{-15}$	(0.00457)
(047) ₃	1		$2\tau^{-13}$	(0.00384)
(047) ₄	1		τ^{-15}	(0.00073)
(057) _p		0.01616	$2\tau^{-10}$	(0.01626)
(057) ₃	2		$2\tau^{-11}$	(0.01005)
(057) ₄	1		τ^{-12}	(0.00311)
(057) ₅	2		τ^{-12}	(0.00311)
(067) _p		0.02550	$2\tau^{-10} + 3\tau^{-12}$	(0.02558)
(067) ₄	1		$2(\tau^{-10} + \tau^{-12})$	(0.02247)
(067) ₅	1		τ^{-12}	(0.00311)
(077) ₅ ^b	2	0.16110	$\tau^{-4} + 3\tau^{-11}$	(0.16097)

^a"Nonperfect" (077)₅ sites.

^b"Perfect" (077)₅ sites [same arrangement of neighbors as in nonperfect (077)₅ site].

quent environments, 472 136 additional points were generated, restricted to the “perfect twelfthfold” sites. The latter were found to include all the sites with $(\alpha\beta'\gamma')=(0\beta''7)$, except that some (077) sites are “imperfect.” To calculate the frequencies of the $(0\beta''7)_p$ sites which differ only in p , the following fact was used: The b'' neighbors among twelfthfold sites are distributed exactly like the b neighbors among the 3D PT vertices. Consequently, the values of $n((0\beta''7)_p)$ in the lower rows of Table VII can be read off from the values of $n((12\beta 0)_p)$ in the lower rows of Table III.

From Table VII, the average values of the “coordination” are $\bar{\alpha}=2\tau^{-5}\cong 0.180$, $\bar{\beta}''=6+2\tau^{-3}\cong 6.472$, and $\bar{\gamma}'=6-2\tau^{-7}\cong 5.931$; thus the average “coordination” number is

$$\bar{Z}=12+4\tau^{-4}\cong 12.584, \quad (19)$$

which is similar to the value (16) for 3D PT vertices.

It is interesting to view the twelfthfold sites as a decoration of the rhombohedra of the τ^3 -inflated 3D PT, as in Fig. 16. Every face is decorated the same way, with one site dividing the long face diagonal in the ratio $\tau^{-1}:\tau^{-2}$. There are two types of P rhombohedra: a fraction τ^{-1} have no interior vertices, while a fraction τ^{-2} have a site [typically, perhaps always of type $(054)_3$ or $(064)_3$], dividing the threefold axis in the ratio $\tau^{-3}:\tau^{-2}$. The O rhombohedra are all the same and each has one short a bond (note the threefold axis is a c bond). The decoration of the faces defines a set of matching rules for packing rhombohedra (one must add the restriction that two neighboring P rhombohedra cannot both have interior sites in the ends near their shared tip vertex).

In the twelfthfold superstructure, the short separations are the a bonds. In contrast to the case of Sec. III, they cannot form chains since $\alpha \leq 1$. Close neighbors can only form isolated pairs. It is interesting to note that these pairs of close twelfthfold sites correspond one-to-one with the closed rings of 10 c bonds discussed in the preceding section—the a bond is, in fact, the symmetry axis at the center of the ring.

In Fig. 17, I show the environment of a site having a close (a) neighbor in the twelfthfold superstructure.⁴⁸

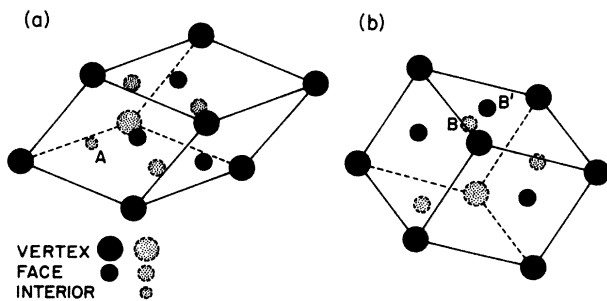


FIG. 16. (a) Prolate and (b) oblate rhombohedra from the τ^3 -inflated 3D PT. Solid circles indicate twelfthfold sites. Vertex, face, and interior sites are distinguished by circle diameter; also, those not on the visible surface are shown dashed and stippled. Note in (a) that the interior site (A) is found in only a fraction τ^{-2} of the prolate rhombohedra. Also, note the short a bond BB' in (b). This figure should be compared with Fig. 8 of Ref. 7.

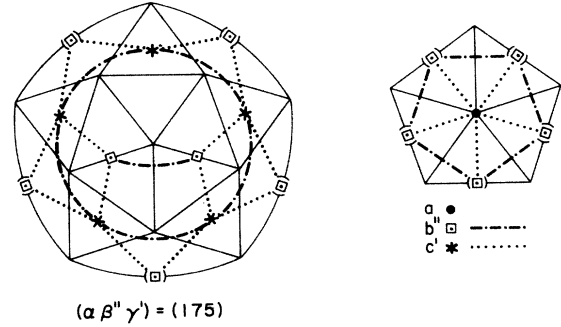


FIG. 17. Environment of a site with a close neighbor in the “superlattice” of twelfthfold sites, projected as in Fig. 14.

B. Sphere packing on twelfthfold sites

There are relatively few a bonds in the “superstructure” of twelfthfold sites, so we can pack spheres of radius $D=c'\cong 2.38$ in most sites. This “twelfthfold” sphere packing has close relations to some interesting physical models described in Sec. V. To construct it, we need only ensure that, for every close pair of sites, exactly one is vacant. This can be accomplished by taking the points represented in pseudospace by the acceptance domain \mathcal{S}_{12} shown in Fig. 9(b); it is produced by removing folded “caps” around each of the 12 fivefold vertices of the triacontahedron \mathcal{C}_{12} . To construct \mathcal{S}_{12} , we take \mathcal{C}_{12} , and, for each fivefold axis \hat{e}_i^\perp , we draw lines through \mathcal{C}_{12} parallel to that axis. Where the intersection of the lines and \mathcal{C}_{12} is longer than one unit, we only include in \mathcal{S}_{12} a centered sub-segment of unit length. We have now ensured that for each i ,

$$\mathcal{S}_{12} \cap (\mathcal{S}_{12} - \hat{e}_i^\perp) = \emptyset, \quad (20)$$

which (recall Sec. III B) shows that there are no accepted points separated by \hat{e}_i in physical space.

This sphere packing occupies all of the twelfthfold sites except exactly half of the $(175)_5$ sites, i.e. (see Table VII), a fraction

$$\tau^{-6} - \tau^{-11} \cong 0.05070 \quad (21)$$

of all 3D PT vertices is occupied. Hence the packing fraction is

$$f = (\pi c'^3/6)(\tau^{-6} - \tau^{-11})/\bar{V} \cong 0.5535 \quad (22)$$

which is much smaller than the packing fraction in Eq. (18).

After the close neighbors are eliminated, most sites in the twelfthfold packing have “coordination” $Z=12$, about 30% of them have $Z=10$ or $Z=11$, and a small number have $Z=7, 8$, or 9 . This reflects the existence of octahedra and larger voids in the structure (which, however, are too small to admit another sphere).

The “unit” and “twelfthfold” sphere packings are *unique* in a sense which I will now explain. Imagine we take the 3D PT acceptance domain \mathcal{C} and continuously shrink its diameter D_1 , monitoring the resulting (progressively sparser) patterns of vertices. At the start we have, after the deletions discussed in Sec. III, the unit sphere

packing (a rather good one) with sphere diameter $D = 1$. As we decrease D_{\perp} the vertices have a decreased density ($\propto D_{\perp}^3$), but there is still an appreciable number of neighbors at distances $a = 1$ and $b' \cong 1.70$. Thus we must maintain $D = 1$ and consequently the packing fraction decreases with the density. It is only after D_{\perp} is reduced by a factor $\sim \tau^{-2}$ that most of the a and b' neighbors go away, allowing the "twelvefold" packing based on b'' and c' neighbors with $D \cong 2.38$. In turn, the b'' and c' neighbors are eliminated after a further reduction of D_{\perp} by $\sim \tau^{-1}$, which gives a packing based on the "perfect twelvefold" sites. However, this is just a τ^3 inflation of the original unit sphere packing.

This does *not* show that these packings have the optimal packing fractions if our only condition is that sphere centers be vertices of the Penrose tiling. In the limit $D \gg a$, one could approximate a random (or fcc) close packing arbitrarily well by the appropriate selection of 3D PT sites. Then the packing fraction could approach that of fcc close packing, $f_{\text{fcc}} \cong 0.7405$. However, the acceptance domain would then become a complex tissue of interleaving tongues or layers of accepted and rejected sectors, rather than the simply connected, nearly convex acceptance domains \mathcal{S}_1 and \mathcal{S}_{12} .

V. RELATIONS OF 3D PENROSE TILING SPHERE PACKINGS TO OTHER MODELS

Icosahedral structures have been modeled theoretically in two (related) fashions. The first approach uses an order parameter $\rho(\mathbf{x})$ which is assumed to be a sum of density waves^{6,7,31,53-55} (related by icosahedral symmetry), such as

$$\rho(\mathbf{x}) = \sum_{i=1}^6 \cos(k_0 \hat{\mathbf{e}}_i \cdot \mathbf{x} + \phi_i), \quad (23)$$

where the phases $\{\phi_i\}$ may be chosen arbitrarily. Equation (23) is known as the "vertex" density-wave pattern^{7,24} since the wave vectors $k_0 \hat{\mathbf{e}}_i$ point in the vertex directions of the reference icosahedron. The main interest was in the Landau theory of the freezing and the microscopic interpretation was entirely unclear. [Is $\rho(\mathbf{x})$ the density of electrons,¹⁵ of atoms,¹³ or of some clusters of atoms?] However, others have put objects on maxima of the density waves, thereby generating sphere packings.^{13,15,56}

The second approach uses discrete and identical tiles,^{3,4,8-10,25-29} it has been used in this paper. Recently an improved density-wave theory has bridged the gap between the two approaches by producing a $\rho(\mathbf{x})$ which can be interpreted as a projection from six dimensions with partial or full occupation of various sites,⁷ closely related to the 3D PT. Here I try to complete the connection by identifying each density-wave model with a corresponding 3D PT sphere packing. Reference 56 turns out to be the unit sphere packing, while the rest^{7,13,15,53} are the twelvefold sphere packing. I will conclude the section by discussing the relation of sphere packings to a model which almost certainly describes the local order in Al-transition-metal quasicrystals.^{8,9}

A. "Vertex" wave patterns and sphere packings

Given a packing constructed by placing spheres upon the strongest maxima of (23), Appendix C implies that we can find an acceptance domain \mathcal{S} which selects a subset of 3D PT points forming essentially the same sphere packing (differing only by small displacements of the sphere centers). The edge length of the 3D PT is given by

$$a = \pi/k_0. \quad (24)$$

The domain \mathcal{S} is roughly spherical (like those of the "unit" or "twelvefold" sphere packings of the preceding sections); we can determine its diameter, since we know that the density of sphere centers is proportional to the volume of \mathcal{S} in pseudospace.⁴²

For example, consider the icosahedral packing of Mercier and Levy⁵⁶ (before it is relaxed under interatomic potentials). In their units $k_0 = 13.85$, $D = 0.96$; this gives $a = \pi/k_0 \cong 0.227$ units, so $D/a = 4.23$, or almost precisely τ^3 . Thus their structure should be, very nearly, the unit sphere packing on a τ^3 -inflated 3D PT. A comparison of their packing fraction $f \cong 0.60$ and their radial distribution function⁵⁶ (see their Figs. 10 and 14) to my Eq. (13) and Fig. 11(a) confirms this identification. [Intriguingly, one planar cut of their packing (their Fig. 1) has a striking resemblance to the 2D PT disk packing of Socolar and Steinhardt,²⁹ while another cut (their Fig. 2) seems identical to variation 2 of the "unit" disk packing of Sec. II C.]

Watson and Weinert¹³ defined another structure based on (23) and intended as a model of real $i(\text{Al-Mn})$. They chose the wave vector which is strongest in x-ray diffraction,² namely $k_0 = 2.896 \text{ \AA}^{-1}$, or $a = 1.085 \text{ \AA}$. Then they fill possible sites by atoms up to the real alloy's density of one atom per 15.1 \AA^3 , i.e., [see Eq. (12)], 0.060 atoms per site of the 3D PT of edge a . This occupied fraction is close to (but somewhat greater than) that of the twelvefold sphere packing, Eq. (21).

Furthermore, they designated a fraction 0.14 of the atoms to be Mn, locating them on the sites of lowest coordination number. In the projection-method picture, it turns out that about half the Mn atoms are on $(\alpha\beta\gamma'') = (0\beta'7)$ sites with $\beta' \leq 6$ (these comprise about $\frac{1}{3}$ of the "inflated" vertex sites of Fig. 16). These correspond in pseudospace to \mathbf{x}^{\perp} close to the center of the acceptance domain. The rest of the Mn atoms occupy sites such as (054) , (055) , and (064) , which have \mathbf{x}^{\perp} close to the edge of the acceptance domain.

For comparison, note that the (probable) real structure⁸⁻¹⁰ corresponds to *all* Mn atoms being on vertex sites. This would give an Mn-Mn pair distribution function like Fig. 11(a) (with $a = 4.60 \text{ \AA}$). Such a pair distribution is closer to that of known Al-Mn alloys in that it lacks the nearest-neighbor Mn-Mn pairs found in the model of Ref. 13.

Straley¹⁵ has performed a Monte Carlo annealing to find stable states of a system of mutually repelling particles (one type only) which also feel an external potential of form (23). The wave vector k_0 and the density are taken from $i(\text{Al-Mn})$ in the same way as Ref. 13. It is clear that the atoms must find the deepest minima of (23); the repulsions (provided they are not too strong) merely ensure that

each site is singly occupied. The resulting structure, therefore, must be very similar to that of Ref. 13, and hence to the twelfold sphere packing.

B. Sachdev-Nelson structure

Sachdev and Nelson⁷ have used an (atomic) density-functional approach to find a metastable structure for hard spheres with the 3D PT symmetry. This is related to the twelfold packing (see below) and has an intriguing resemblance to the atomic decoration in the $i(\text{Al-Mn-Si})$ structure;⁹ however, the existence of two different simple sphere packings on the 3D PT suggests that the assumptions of the density-functional theory should be reexamined to see how robust its results are.

Their theory is formulated in terms of a density $\rho(\mathbf{x}, \mathbf{x}^\perp)$ defined in six-dimensional space; the physical density is a section taken at constant \mathbf{x}^\perp . [This is the same notion as Eqs. (C1) and (C2), but now generalized to include higher harmonic wave vectors.] Roughly speaking, one seeks that $\rho(\mathbf{x}, \mathbf{x}^\perp)$ which gives a physical density, the radial distribution function of which must closely approximate⁷ that of a random close packing of spheres^{19,20} (or an elemental metallic glass^{23,24}). As it turns out, the 6D density is well represented by

$$\rho(\mathbf{x}, \mathbf{x}_0^\perp) = \sum_{[n]} \rho_\perp(\mathbf{x}_0^\perp - \mathbf{x}_{[n]}^\perp) \rho_{||}(\mathbf{x} - \mathbf{x}_{[n]}), \quad (25)$$

where $\mathbf{x}_{[n]}^\perp$ and $\mathbf{x}_{[n]}$ are given by (7) and (8), and both $\rho_\perp(\dots)$ and $\rho_{||}(\dots)$ are Gaussians.⁷ The physical space Gaussians $\rho_{||}(\dots)$, which represent thermal vibrations,⁷ are rather sharp; they can reasonably be replaced in (26) by δ functions centered on 3D PT sites, giving

$$\rho(\mathbf{x}, \mathbf{x}_0^\perp) = \sum_{[n]} \rho_\perp(\mathbf{x}_0^\perp - \mathbf{x}_{[n]}^\perp) \delta(\mathbf{x} - \mathbf{x}_{[n]}) \quad (26)$$

which describes a zero-temperature structure. This can be viewed as a generalization of the projection construction (Sec. III A), in which the boundaries of the acceptance domain \mathcal{S} become fuzzy. [In other words, the acceptance function $\chi_\perp(\dots)$ of Eq. (C3), which only takes the values 0 or 1, is replaced in (26) by the continuous function $\rho_\perp(\dots)$.] Sachdev and Nelson⁷ interpret $\rho_\perp(\mathbf{x}_0^\perp - \mathbf{x}_{[n]}^\perp)$ as a partial (statistical) occupation of site $\mathbf{x}_{[n]}$.

Now, in fact, the Sachdev-Nelson structure has a density of occupation ~ 0.060 spheres per 3D PT site, similar to (21), and its ball size is $D \cong 2.5a$. Thus, this packing is an approximation to the “twelfold” packing. Compare Fig. 16 to their Fig. 8.

Sachdev and Nelson’s computation allowed variation of the ratio D/a to minimize the density-functional free energy. It is somewhat surprising that the density-functional calculation selects the twelfold sphere packing, with its low density, over the “unit” sphere packing. There are two possible explanations.

(i) Possibly Fig. 11(b) is a better approximation than Fig. 11(a) to the radial distribution function of random close packing.

(ii) The acceptance domain \mathcal{S}_{12} [Fig. 9(b)] is very nearly spherical; on the other hand, the corresponding domain \mathcal{S}_1 for the “unit” sphere packing extends out much far-

ther in fivefold directions than in twofold directions. Since the calculation of Ref. 7 assumed $\rho_\perp(\mathbf{x}_1^\perp)$ was a spherically symmetric Gaussian, it might find it easier to approximate the acceptance function of \mathcal{S}_{12} than that of \mathcal{S}_1 .

One should note in any case that the density-functional calculation is not very sensitive to the packing fraction. Although the density is constrained to be equal to that for the random-close-packed structure, the model allows occupations $\rho_\perp(\mathbf{x}^\perp)$ greater than unity of single sites, as well as clusters of mutually inconsistent sites with combined occupation greater than unity. These excess occupations compensate for the excessive voids. Possibly a different scale would be selected by an improved model. This could mean allowing more general forms of $\rho_\perp(\mathbf{x}^\perp)$, forcing $\rho_\perp(\mathbf{x}^\perp) \leq 1$, or taking into account correlations between occupancies of neighboring sites.

C. Sphere packings and the $i(\text{Al-Mn-Si})$ structure

Another packing which seems closely related to the twelfold sphere packing is described in Refs. 8 and 9. The structures of the crystalline alloys $\alpha(\text{Al-Mn-Si})$ and $\alpha(\text{Al-Fe-Si})$ are described by (respectively) bcc and hexagonal packings of 54-atom Mackay icosahedra (MI’s), which are practically spherical clusters with $D \cong 11.6$ Å. The α phases can also be described as (periodic) packings of 3D rhombohedral Penrose tiles, with the Mn (or Fe) atoms at vertices; in this description the centers of the MI’s sit on twelfold-type vertices. Furthermore, in these structures the centers of two neighboring MI’s are separated by either b'' - or c' -type displacements; the centers are (respectively) at the tips of a rhombic dodecahedron (RD) or a P rhombohedron. The same thing seems to be true of the 3D PT, from inspection of a finite realization; that is, b'' or c' separations between twelfold sites are usually (but not always) spanned by an RD or a P .

Since $\alpha(\text{Al-Mn-Si})$ and $\alpha(\text{Al-Fe-Si})$ have atomic structures closely related to the icosahedral alloys $i(\text{Al-Mn})$ and $i(\text{Al-Mn-Si})$,^{8,9} this suggests a model for the latter structures in which MI clusters are placed on sites of the twelfold sphere packing. Three kinds of icosahedral order coexist in the structure: (i) orientational (the MI clusters are all aligned the same way), (ii) bond orientational (of the bond vectors between neighboring MI’s), and (iii) translational (which give rise to the sharp diffraction peaks.^{1-6,41,42} For the MI, a relationship of (i) and (ii) propagates a long-range order in (iii). Any Landau theory that can adequately represent this ordering mechanism must have (i) an order parameter $\rho(\mathbf{x})$ representing a density of MI units (not of atoms), and (ii) orientational or bond-orientational order parameters⁵⁵ to account for the different kinds of order.

Although the model of $i(\text{Al-Mn-Si})$ as a decorated sphere packing is attractive, one should be cautious about taking it too seriously, for two reasons. (i) The packing fraction (20) is much less than that for a bcc lattice [i.e., $\alpha(\text{Al-Mn-Si})$], $f_{\text{bcc}} \cong 0.68$. (ii) It is hard to believe that an alloy formed only by rapid quenching can develop the subtle long-range translational correlations of a defect-free quasicrystal.

VI. SUMMARY

I have presented many facts, methods, and statistics that will be useful for models of icosahedral and pentagonal structures. In particular, methods were given in Secs. III and IV and in Appendixes A and B, for using the "projection" technique to find any desired information about the distribution of local environments or other patterns.

Three kinds of good packing have been displayed: the unit disk packing (and its pentagon variant) in Sec. II, the unit sphere packing in Sec. III D, and the twelfefold sphere packing in Sec. IV B. As noted in Sec. IV B, there are no other good sphere packings described by a 6D projection with a simple acceptance domain. The disk and sphere packings exhibited have shown that simple Penrose-tiling based structures are not excessively loose; in fact, it is conceivable that for packings with several sizes of sphere, there are some diameter ratios for which a Penrose-tiling packing, using a mixture of sizes, might give a better packing fraction than a mixture of ordinary close-packed domains.

I have described how these packings are related to previous physical models. The unit disk packing was related to the Al_3Fe atomic structure^{10,14} (Secs. II B 2 and II B 4) and to other 2D PT models.^{12,25-29} Atom decoration schemes describing the $i(\text{Al-Mn})$ and $i(\text{Al-Zn-Mg})$ structures⁹⁻¹¹ were related to the unit sphere packing (Sec. III D) and the twelfefold sphere packing (Sec. IV B). Finally, the density-wave models^{6,7,53-56} were related to both sphere packings (Sec. V, and Appendix C).

Note added in proof. Kumar *et al.*⁵⁷ have an independent treatment of 2D PT very similar to my Sec. II. Further discussions of the relations between tilings, density-wave patterns, and other structures with continuously varying displacements $\mathbf{u}(\mathbf{u}^+)$ (cf. Appendix C and Ref. 54) have appeared.^{58,59}

ACKNOWLEDGMENTS

I am indebted, for helpful conversations, to D. R. Nelson, P. Wolynes, D. Levine, S. Sachdev, D. P. DiVincenzo, and especially Veit Elser, who taught me the mathematics of quasilattices. I thank the latter three and also M. A. Marcus, for thoughtful comments on the manuscript. I am grateful for financial support by IBM. Work at Cornell University was also supported by the National Science Foundation under Grant No. DMR-8314625.

APPENDIX A: 2D PENROSE TILING CONSTRUCTED BY PROJECTION

The projection method is an alternative means to "deflation" for constructing the 2D PT. I outline it here for purposes of exposition: some concepts which appear in applying the 3D PT construction (Sec. III) are more easily visualized and represented in the 2D case. This discussion assumes previous exposure of the reader to the projection

method (as presented for the 3D PT).^{5,6,41,42} [Also, other descriptions of the 2D PT projection may be found in Refs. 31, 32, and 33(b).]

Real quasilattice vertices $\mathbf{x}_{[n]}$ and pseudospace vertices $\mathbf{x}_{[n]}^\perp$ are defined just as in Eqs. (6) and (7); however, we omit one of the $\hat{\mathbf{e}}_i$'s so that points are now indexed by $[n] = [n_1, n_2, \dots, n_5]$. Thus, we still picture real space and pseudospace as three dimensional. (By the end, both the pseudospace lattice of included $\{\mathbf{x}_{[n]}^\perp\}$ and the physical space lattice will reduce to essentially two-dimensional objects.)

We should include a vertex $\mathbf{x}_{[n]}$ whenever the corresponding $\mathbf{x}_{[n]}^\perp$ is in \mathcal{C}_5 , the projection [analogous to (9)] of the 5D hypercubic unit cell; this turns out to be a rhombic icosahedron [Fig. 18; compare Fig. 9(a)]. The fivefold (vertical) axis $\hat{\mathbf{z}}^\perp$ is chosen parallel to the omitted $\hat{\mathbf{e}}_k$ in pseudospace. Similarly, $\hat{\mathbf{z}}$ is chosen parallel to the omitted $\hat{\mathbf{e}}_k$ in physical space; the edges connecting vertices lie along the remaining icosahedral ($\hat{\mathbf{e}}_i$) directions.

Now, note that all the remaining $\hat{\mathbf{e}}_i^\perp$ have vertical components $\pm 1/\sqrt{5}$ so that the set $\{\mathbf{x}_{[n]}^\perp\}$ defined by Eq. (8) uniformly fills a set of planes³¹ spaced by $1/\sqrt{5}$ (instead of uniformly filling space as in the 3D PT case). The points included in the 2D PT lie in the intersection of these planes and the rhombic icosahedron \mathcal{C}_5 . Since the latter has an axis of length $\sqrt{5}$, we get five levels in the intersection for a generic choice of \mathbf{x}_0^\perp .

In real space, if we choose $\hat{\mathbf{z}}$ parallel to the omitted $\hat{\mathbf{e}}_k$, then by (6) all the remaining $\hat{\mathbf{e}}_i$ have $(\hat{\mathbf{e}}_i)_z = -(\hat{\mathbf{e}}_i^\perp)_z$, so the physical points also lie in equally spaced layers corresponding one-to-one to those in pseudospace. Since only a few levels in pseudospace have any included points, the physical space levels are similarly restricted. In fact the physical points form a Wieringa roof,³² a surface which can be projected flat to make a tiling of Penrose rhombi (see Sec. II B 2).

One can go through the tiling of Penrose rhombi label-

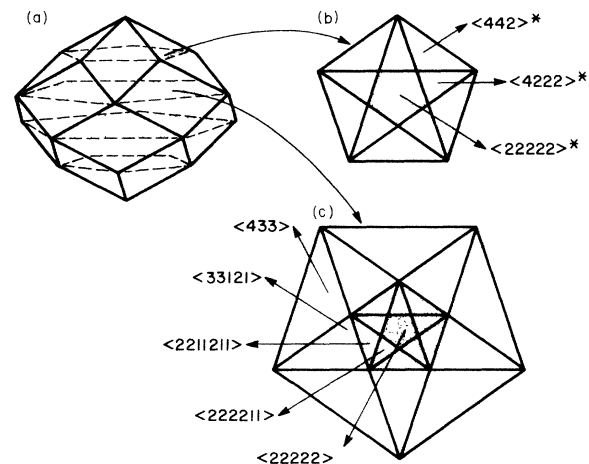


FIG. 18. Acceptance domain in construction of 2D PT by projection. (a) The rhombic icosahedron \mathcal{C}_5 in pseudospace. (b) and (c) Views of two layers in \mathcal{C}_5 showing division into sectors, labeled by the corresponding vertex type. [The other two layers are 180° rotations of (c) and (b).] Shaded sectors correspond to "fivefold" sites.

ing alternate vertices “even, odd, even, . . .” since each tile has an even number of edges, this is well defined. Then the levels in pseudospace correspond alternately to all even and all odd points. The genuine Penrose tiling (which satisfies the matching rules) has equal numbers of “even” and “odd” points; this forces a choice of \mathbf{x}_0^\perp , which gives the symmetrical set of four pentagonal levels shown in Fig. 18(a). The top and bottom layers [Fig. 18(b)] correspond to even and odd “pole” sites, while the middle layers [Fig. 18(c)] correspond to odd and even “nonpole” sites. Note how the sharp distinction of “pole” and “nonpole” sites (which makes it simple to define matching rules) arises because the domain of included $\{\mathbf{x}_{[n]}^\perp\}$ is disconnected. (In the 3D PT case, the domain \mathcal{C} is connected and no sharp division is possible.)

Sectors corresponding to the eight vertex types of Fig. 3 are indicated in Figs. 18(b) and 18(c); note an equivalent picture appears in Figs. 8 and 9 of Ref. 32. If we distinguish different orientations of the same vertex, we find a total of 64 sectors. Note that, of the ten possible orientations of a typical vertex, five are found only at even vertices and five only at odd vertices. (The 3D PT can also be divided into even and odd sublattices, but each sublattice contains every possible orientation of every vertex type.)

It is interesting to consider point sets defined by using subdomains: if we include only points from the middle layers [Fig. 18(c)], we get the “unit” disk packing variation (ii). The series of pentagons highlighted by shadings in Figs. 18(b) and 18(c), each smaller by a factor τ , corresponds to the succession of inflations mentioned in Sec. II A.

APPENDIX B: CALCULATION OF 3D PENROSE TILING VERTEX FREQUENCIES

Here I present the proofs and details of the methods used for the results in Sec. III C.

1. Directions of (a, b, c) neighbors are equivalent to packing arrangement of rhombohedron corners at a vertex: proof

Imagine we are given (i) a packing of the shapes in Fig. 13 over a reference icosahedron, in which everything has been erased except (ii) the points indicating a , b , and c neighbors: Can we uniquely reconstruct the packing of the solid angle? We can immediately locate all the O_7 corners from the c bonds. In the remaining part of the reference icosahedron, any icosahedron vertex that does *not* have an a neighbor over it must be in the interior of the projection of a P_3 corner; the orientation of this P_3 corner on the icosahedron is determined since, of the five icosahedron edges radiating from this empty vertex, exactly two will have b neighbors over them [see Fig. 13(b)]. Any remaining icosahedron-face triangles without any b neighbors over their edges must be P_1 corners [see Fig. 13(a)] and what is left over can be divided up into O_1 corners. The converse—that the packing of the corners determines the arrangement of Voronoi neighbors—was demonstrated in Sec. III B (see Fig. 12).

2. Numbers of (a, b, c) neighbors are equivalent to numbers of rhombohedron corners at a vertex: proof

This is not equivalent to the preceding proof: given a set of corners, there are many ways to pack them around a vertex. Here I show that each of these (including those which are not allowed in the 3D PT) must have the *same* numbers $(\alpha\beta\gamma)$ of neighbors. For, given the numbers of corners of each type, $N(P_1)$, $N(P_3)$, $N(O_1)$, and $N(O_7)$, we have

$$\begin{pmatrix} \alpha \\ \beta \\ \gamma \\ 1 \end{pmatrix} = \begin{pmatrix} \frac{3}{5} & \frac{4}{5} & \frac{3}{5} & \frac{6}{5} \\ 0 & 1 & \frac{1}{2} & \frac{3}{2} \\ 0 & 0 & 0 & 1 \\ \frac{1}{20} & \frac{3}{20} & \frac{1}{20} & \frac{7}{20} \end{pmatrix} \begin{pmatrix} N(P_1) \\ N(P_3) \\ N(O_1) \\ N(O_7) \end{pmatrix}. \quad (\text{B1})$$

The first three rows come from apportioning bonds which are shared between corners; for instance, a P_3 corner (see Fig. 13) has two a neighbors with a $\frac{3}{10}$ share in each and one with a $\frac{1}{5}$ share for a total of $\frac{4}{5}$, plus two b neighbors with a $\frac{1}{2}$ share in each for a total of 1. The last row comes because the solid angle must add up to 4π .

The matrix in (B1) can be inverted as

$$\begin{pmatrix} N(P_1) \\ N(P_3) \\ N(O_1) \\ N(O_7) \end{pmatrix} = \begin{pmatrix} 1 & -2 & -1 & 8 \\ -1 & 0 & -3 & 12 \\ 2 & 2 & 3 & -24 \\ 0 & 0 & 1 & 0 \end{pmatrix} \begin{pmatrix} \alpha \\ \beta \\ \gamma \\ 1 \end{pmatrix} \quad (\text{B2})$$

and this proves the equivalence of $(\alpha\beta\gamma)$ and $(N(P_1), \dots)$.

3. Analytic calculation of vertex frequencies

A “numerological” method was described in Sec. III B for (reliably) guessing the exact frequencies of each vertex class of the 3D PT. Here I present the direct approach: determining the coordinates, and then calculating the volume, of each sector within the acceptance domain, the triacontahedron \mathcal{C} . This confirms the “numerological” results.

A motivation for this calculation is that, in realistic structural models of quasicrystals,^{9,10} vertices are decorated by different types (or different arrangements) of atoms, according to their vertex type. Calculation of the diffraction patterns of such models requires an integration over pseudospace,⁴²

$$\int_{\mathcal{C}} d^3\mathbf{x}^\perp e^{i\mathbf{q}^\perp \cdot \mathbf{x}^\perp} F(\mathbf{q}, \mathbf{x}^\perp), \quad (\text{B3})$$

where $(\mathbf{q}, \mathbf{q}^\perp)$ are the physical and pseudo components of the wave vector, and $F(\cdot, \mathbf{x}^\perp)$ is the form factor for the decoration of a vertex corresponding to \mathbf{x}^\perp . Any analytic evaluation of (B3) requires knowledge of the sector locations and boundaries.

In mapping out the sectors, it was very useful to know which sectors shared faces with each other. This information is presented in Table VIII: the sectors adjoin in \mathcal{C} if their entries do in Table VIII. [The relationships in Table VIII were determined by examining pictures of the environments⁴⁸ and determining which ones differed by addi-

TABLE VIII. Relationships between 3D PT site types.

(670) ₅	(561) ₄	(452) ₃			
(770) ₅	(661) ₄				
(870) ₅					
(970) ₅	(960) ₄				
(1070) ₅	(1060) ₄	(1050) ₃			
(1270) ₅	(1260) ₄	(1250) ₃			
(1260) ₅	(1250) ₄	(1240) ₃	(1230) ₂		
(1250) ₅	(1240) ₄	(1230) ₃	(1220) ₂	(1210) ₁	(1200) ₀

tion of one neighbor—which must always be a (452) neighbor.] It was also helpful in mapping the sectors to have the symmetry numbers s from Table III, e.g., if a vertex has threefold symmetry $s=3\cdot 2$, its sector must have the same symmetry and lie on the corresponding pseudospace symmetry axis in \mathcal{C} .

The sectors are convex polyhedra; their vertices are given in Tables IX and X. In Table IX, s labels the symmetry of each point using the same convention as Table III. Note that I suppress a factor of $(\tau\sqrt{5})^{-1/2}$ in all the coordinates. For convenience, a coordinate system is chosen so that $(\hat{x}\hat{y}\hat{z})$ are oriented on icosahedral 2×2 axes, so the icosahedral vectors $\pm\hat{e}_i$ have coordinates $(0, \pm 1, \pm\tau)$ plus cyclic permutations. I only consider the parts of sectors within one asymmetric unit \mathcal{C}_A of \mathcal{C} , which is bounded by points 0, 18, 19, and 20. The points 2, 7, 9, and 11 come only from the intersections with planes bounding the asymmetric unit. Note also that points 1–3 lie on the surface of the inner (1200) triacontahedron, points 6 and 10–13 are on the surface of \mathcal{C}_{12} , and points 18–20 are on the surface of \mathcal{C} . It is now trivial to calculate the fraction of \mathcal{C}_A occupied by each sector in Table X. The results agree with the last column of Table III.

TABLE IX. Vertices of sectors in pseudospace.

Label	Coordinates	Symmetry s
0	(0,0,0)	$2^3\cdot 3\cdot 5$
1	$(0, \tau^{-2}, \tau^{-1})$	2·5
2	$(0, 0, \tau^{-1})$	2·2
3	$(\tau^{-3}, 0, \tau^{-1})$	2·3
4	$(0, 0, 2\tau^{-2})$	2·2
5	$(\tau^{-4}, \tau^{-3}, 2\tau^{-2})$	2
6	$(\tau^{-2}, 0, 1)$	2·3
7	$(0, \tau^{-3}, 2\tau^{-2})$	2
8	$(0, \tau^{-3}, \tau^{-1} + \tau^{-3})$	2
9	$(\tau^{-3}/2, \tau^{-1}/2, \tau^{-1} + \tau^{-2}/2)$	2
10	$(0, \tau^{-4}, 1)$	2
11	(0,0,1)	2·2
12	$(\tau^{-3}, \tau^{-3}, 1)$	2
13	$(0, \tau^{-1}, 1)$	2·5
14	$(0, 0, 2\tau^{-1})$	2·2
15	$(\tau^{-1}, 0, \tau)$	2·3
16	(0,0,2)	2·2
17	$[\frac{1}{2}, \tau^{-1}/2, (\tau^2+1)/2]$	2
18	$(1, 0, \tau^2)$	2·3
19	$(0, \tau, \tau^2)$	2·5
20	$(0, 0, \tau^2)$	2·2

APPENDIX C: RELATIONSHIP OF DENSITY-WAVE PATTERNS AND PROJECTION METHODS

Here I show how sphere packings made from density-wave patterns,^{7,13,15,31,53,56} such as Eq. (23), correspond to those made by projection. (This correspondence has already been discussed in Refs. 7 and 56.)

Equation (23) can be rewritten as

$$\rho(\mathbf{x}) = \sum_{i=1}^6 \cos[k_0 \hat{e}_i \cdot (\mathbf{x} - \mathbf{x}_0) - k_0 \hat{e}_i^\perp \cdot \mathbf{x}_0^\perp]. \quad (\text{C1})$$

So far $(\mathbf{x}_0, \mathbf{x}_0^\perp)$ are just an alternative way to parametrize the six independent phases of the density waves. However, writing

$$\rho(\mathbf{x}, \mathbf{x}^\perp) \equiv \sum_{i=1}^6 \cos[k_0 \hat{e}_i \cdot (\mathbf{x} - \mathbf{x}_0) + k_0 \hat{e}_i^\perp \cdot (\mathbf{x}^\perp - \mathbf{x}_0^\perp)] \quad (\text{C2})$$

we see that (C1) is just a three-dimensional section taken at $\mathbf{x}^\perp=0$ through a density (C2) in the six-dimensional space of $\{\mathbf{x}, \mathbf{x}^\perp\}$. (This is illustrated in Ref. 54.)

TABLE X. Sectors in pseudospace.

Site type	Labels of corners of sector
(1200) ₀	(0,1,2,3)
(1210) ₁	(1,2,3,4)
(1220) ₁	(1,3,4,5)
(1230) ₂	(3,4,5,6)
(1230) ₃	(1,5,7,8)
(1240) ₃	(4,5,6,8)
(1240) ₄	(1,5,8,9)
(1250) ₃	(4,6,8,10,11)
(1250) ₄	(5,6,8,9,12)
(1250) ₅	(1,8,9,13)
(1260) ₄	(6,8,10,12)
(1260) ₅	(8,9,12,13)
(1270) ₅	(8,10,12,13)
(1050) ₃	(6,10,11,14)
(1060) ₄	(6,10,12,14)
(1070) ₅	(10,12,13,14)
(960) ₄	(6,12,14,15)
(970) ₅	(12,13,14,15)
(870) ₅	(13,14,15,16)
(770) ₅	(13,15,16,17)
(670) ₅	(13,16,17,19)
(661) ₄	(15,16,17,18)
(561) ₄	(16,17,18,19)
(452) ₃	(16,18,19,20)

Furthermore, the density (C2) has the periodicities of a 6D simple cubic lattice generated by six orthogonal vectors $\{a(\hat{e}_i, \hat{e}_i^\perp)\}$ of length $\sqrt{2}a$. Here $k_0 = \pi/a$. (I have generally taken $a=1$, without loss of generality.)

A set of points $\{\mathbf{x}_{[n]}\}$ defined by projection [Eq. (8)] using some acceptance domain \mathcal{S} , can be written as a density

$$\rho(\mathbf{x}) = \sum_{[n]} \chi_{\mathcal{S}}(\mathbf{x}^\perp - \mathbf{x}_{[n]}^\perp) \delta(\mathbf{x} - \mathbf{x}_{[n]}) \quad (\text{C3})$$

with the same periodicities; here $\chi_{\mathcal{S}}(\cdot)$ is the "acceptance function."³¹ $\chi_{\mathcal{S}}(\mathbf{x}^\perp) = 1$ if $\mathbf{x}^\perp \in \mathcal{S}$ and $\chi_{\mathcal{S}}(\mathbf{x}^\perp) = 0$ otherwise.

One converts a density-wave structure into a discrete set of sites (on which spheres may be placed) by selecting local maxima of (C1). I will show that such sets are very similar to projected sets (C3), taken using an appropriate acceptance function. [Since the local maxima of (C2) in 6D space occur at vertices $(\mathbf{x}_{[n]}, \mathbf{x}_{[n]}^\perp)$ of the 6D simple cubic lattice, this is not so surprising.]

When $\mathbf{x}_0^\perp = \mathbf{0}$, then \mathbf{x}_0 is an absolute maximum point of (C1) and is a center of icosahedral symmetry. In general the position \mathbf{x}^* of the local maximum depends parametrically and continuously on \mathbf{x}_0^\perp :

$$\mathbf{x}^*(\mathbf{x}_0^\perp) \equiv \mathbf{x}_0 + \mathbf{u}(\mathbf{x}_0^\perp). \quad (\text{C4})$$

(We choose the branch of solutions of $\nabla\rho(\mathbf{x}) = \mathbf{0}$ which has $\mathbf{u}(\mathbf{0}) = \mathbf{0}$.) To lowest order in \mathbf{u}^\perp ,

$$\mathbf{u}(\mathbf{u}^\perp) \cong \frac{\pi^2}{12} \sum_{i=1}^6 \hat{e}_i (\hat{e}_i^\perp \cdot \mathbf{u}^\perp)^3 \quad (\text{C5})$$

so that, for small \mathbf{u}^\perp , the displacement is very small and $\mathbf{x}^*(\mathbf{u}^\perp)$ is essentially the point \mathbf{x}_0 which would be generated by projection. [Note in (C5) that when \mathbf{u}^\perp is in a symmetry direction in pseudospace, then \mathbf{u} is in the corresponding symmetry direction in physical space.] Inspection of (C2) makes it clear that there will be similar branches near other projected points,

$$\mathbf{x}_{[n]}^*(\mathbf{x}_0^\perp) = \mathbf{x}_{[n]} + \mathbf{u}(\mathbf{x}_{[n]}^\perp - \mathbf{x}_0^\perp) \quad (\text{C6})$$

with the same displacement function $\mathbf{u}(\cdot \cdot \cdot)$.

Of course, we cannot follow the maximum, Eq. (C4), out to arbitrarily large \mathbf{u}^\perp . As \mathbf{u}^\perp moves away from zero (say along a symmetry direction), the amplitude decreases and at a value $\mathbf{u}_{\text{crit}}^\perp$ the maximum bifurcates or splits up

into a ring of weak, nearby minima; as we continue to vary \mathbf{u}^\perp these branches of solutions will similarly reconnect, by some reverse bifurcation, to the branch $\mathbf{x}_{[n]}^*$ from a different $[n]$.

In general, the criterion for accepting a maximum (for placing a sphere) depends upon its amplitude and its local environment (e.g., upon whether there are other maxima nearby). But these are functions of $\mathbf{u}_{[n]}^\perp \equiv \mathbf{x}_{[n]}^\perp - \mathbf{x}_0^\perp$, so we can express the criterion by an acceptance function $\chi(\mathbf{u}^\perp)$:

$$\rho(\mathbf{x}) = \sum_{[n]} \chi(\mathbf{x}_{[n]}^\perp - \mathbf{x}_0^\perp) \delta(\mathbf{x} - \mathbf{x}_{[n]} - \mathbf{u}(\mathbf{x}_{[n]}^\perp - \mathbf{x}_0^\perp)), \quad (\text{C7})$$

where $\chi(\mathbf{u}^\perp) = 1$ for \mathbf{u}^\perp yielding an acceptable maximum, $\chi(\mathbf{u}^\perp) = 0$ otherwise. It is now evident that (C7) describes a subset of 3D PT vertices $\{\mathbf{x}_{[n]}\}$, selected by $\chi(\cdot \cdot \cdot)$, each of which is then displaced by $\mathbf{u}(\mathbf{x}_{[n]}^\perp - \mathbf{x}_0^\perp)$.

What is the sphere packing which most resembles the density-wave pattern (C1) (i.e., the dark regions in Fig. 1(a) of Ref. 53)? It should include *all* of the well-defined maxima, i.e., the "natural" acceptance domain \mathcal{S} should extend out to $(\mathbf{u}_{\text{crit}}^\perp)$. Now the diameters $D_1 = 2|\mathbf{u}_{\text{crit}}^\perp|$ are, respectively, 1.27, 1.52, and 1.00 in the twofold, threefold, and fivefold directions in pseudospace; thus \mathcal{S} has perhaps twice the volume of the acceptance domain of the twelfold" sphere packing (compare Fig. 9 caption). The inclusion of more points (primarily at $b' \cong 1.70$ separations) is the main difference from the twelfold centers; for the maximum displacements from the projected positions, $\mathbf{u}(\mathbf{u}_{\text{crit}}^\perp)$, have magnitudes $\sim 0.16, 0.09$, and 0.50 , respectively, which are small compared to the typical separations between sphere centers in the twelfold packing (2.38 and 2.75). To get to the unit sphere packing we would have to increase the acceptance volume by $\sim \tau^6$, or 20 times that of the twelfold packing; thus, it is reasonable to view the density-wave structure (C1) as a rough approximation to the "twelfold" sphere packing.

Previous authors selected maxima by a somewhat different procedure: They chose the highest (remaining) maxima until they reached a specified density (Ref. 13), or until spheres placed on the maxima started to overlap (Ref. 56). Now, the amplitude of a maximum is a function of \mathbf{u}^\perp which deviates from spherical symmetry only in order $|\mathbf{u}^\perp|^6$. Thus these procedures *also* correspond, in pseudospace, to filling up a nearly spherical acceptance domain (which may be smaller than that of the twelfold sphere packing).

*Present address.

¹D. Schechtman, I. Blech, D. Gratias, and J. W. Cahn, Phys. Rev. Lett. **53**, 1951 (1984).

²P. A. Bancel, P. A. Heiney, P. W. Stephens, A. I. Goldman, and P. M. Horn, Phys. Rev. Lett. **54**, 2422 (1985).

³P. Ramachandrarao and G. V. S. Sastry, Pramana **25**, L225 (1985).

⁴D. Levine and P. J. Steinhardt, Phys. Rev. Lett. **53**, 2477 (1984); Phys. Rev. B **34**, 596 (1986).

⁵V. Elser, Phys. Rev. B **32**, 4892 (1985).

⁶P. A. Kalugin, A. Yu. Kitaev, and L. C. Levitov, Pis'ma Zh. Eksp. Teor. Fiz. **41**, 119 (1985) [JETP Lett. **41**, 145 (1985)]; J.

Phys. (Paris) Lett. **46**, L601 (1985).

⁷S. Sachdev and D. R. Nelson, Phys. Rev. B **32**, 4592 (1985).

⁸P. Guyot and M. Audier, Philos. Mag. B **52**, L15 (1985); M. A. Audier and P. Guyot, Philos. Mag. B **53**, L43 (1986).

⁹V. Elser and C. L. Henley, Phys. Rev. Lett. **55**, 2883 (1985).

¹⁰C. L. Henley, J. Non-Cryst. Solids **75**, 91 (1985).

¹¹C. L. Henley and V. Elser, Philos. Mag. B **53**, L59 (1986).

¹²L. A. Bursill and P. J. Lin, Nature **316**, 50 (1985).

¹³R. E. Watson and M. Weinert, Mater. Sci. Eng. **79**, 105 (1986).

¹⁴C. L. Henley (unpublished).

¹⁵J. P. Straley (unpublished).

- ¹⁶F. C. Frank and J. Kasper, *Acta Cryst.* **11**, 184 (1958); **12**, 483 (1959).
- ¹⁷A. L. Mackay, *Acta Cryst.* **15**, 916 (1962).
- ¹⁸J. A. Barker, *J. Phys. (Paris) Colloq.* **38**, C2-37 (1977); M. Hoare, *Ann. N.Y. Acad. Sci.* **279**, 186 (1976).
- ¹⁹J. D. Bernal, *Proc. R. Soc. London, Sect. A* **280**, 299 (1964).
- ²⁰J. L. Finney, *Proc. R. Soc. London, Sect. A* **319**, 479 (1970); C. H. Bennett, *J. Appl. Phys.* **43**, 2727 (1972).
- ²¹R. Mosseri and J. F. Sadoc, *J. Phys. (Paris) Lett.* **45**, L827 (1984).
- ²²R. Mosseri and J. F. Sadoc, *J. Non-Cryst. Solids* **75**, 115 (1985).
- ²³D. R. Nelson, *Phys. Rev. B* **28**, 5515 (1983).
- ²⁴S. Sachdev and D. R. Nelson, *Phys. Rev. B* **32**, 1480 (1985).
- ²⁵A. L. Mackay, *Physica* **114A**, 609 (1982).
- ²⁶A. L. Mackay, *Kristallografiya* **26**, 910 (1981) [*Sov. Phys.—Crystallogr.* **26**, 517 (1981)].
- ²⁷R. Mosseri and J. F. Sadoc, in *Structure of Non-Crystalline Materials*, edited by P. H. Gaskell, J. M. Parker, and E. A. Davis (Taylor and Francis, New York, 1983).
- ²⁸J. F. Sadoc and R. Mosseri, *J. Non-Cryst. Solids* **61&62**, 487 (1984).
- ²⁹J. E. S. Socolar and P. J. Steinhardt, *Phys. Rev. B* **34**, 617 (1986).
- ³⁰L. Bendersky, *Phys. Rev. Lett.* **55**, 1461 (1985).
- ³¹T. L. Ho, *Phys. Rev. Lett.* **56**, 468 (1986).
- ³²N. G. de Bruijn, *Ned. Akad. Wetensch. Proc. A* **84**, 39 (1981); **84**, 53 (1981).
- ³³(a) M. Gardner, *Sci. Am.* **236** (1), 110 (Jan. 1977). (b) M. V. Jarić, *Phys. Rev. B* (to be published). This includes an independent description of the 2D PT and its local environments, similar in spirit to Sec. II and Appendix A of the present work.
- ³⁴J. Peyrière (unpublished).
- ³⁵If we assign fractions of each vertex to the adjacent rhombi according to the angles they subtend, then each rhombus gets a total of exactly one vertex, which shows that rhombi have the same density as vertices. The same argument (using solid angles) shows that rhombohedra have the same density as vertices in the 3D PT.
- ³⁶J. G. Berryman, *Phys. Rev. A* **27**, 1053 (1983), and references therein.
- ³⁷M. Rubinstein and D. R. Nelson, *Phys. Rev. B* **26**, 6254 (1982).
- ³⁸Z. Zhang, H. Q. Ye, and K. H. Kuo, *Philos. Mag. A* **52**, L49 (1985); see their Fig. 3.
- ³⁹P. W. Stephens and A. I. Goldman (unpublished). (In principle the diffraction peaks have finite widths, but here they were found to be limited by the sample size.)
- ⁴⁰T. S. Baker, D. L. D. Caspar, and W. T. Murakami, *Nature* **303**, 446 (1983).
- ⁴¹M. Duneau and A. Katz, *Phys. Rev. Lett.* **54**, 2688 (1985); A. Katz and M. Duneau, *J. Phys. (Paris) Colloq.* **46**, C8-31 (1985); *J. Phys. (Paris)* **47**, 181 (1986).
- ⁴²V. Elser, *Acta Cryst. A* **42**, 36 (1986).
- ⁴³D. Levine (private communication).
- ⁴⁴I present (11) as a starting point because it is easily remembered and analogous to (4), but it has no direct derivation. One can get (11) by considering the sector in \mathcal{C} (see Sec. III B) corresponding to a given vertex of a P or O rhombohedron of a given orientation: the sector is also P or O rhombohedron (in pseudospace). The frequencies of the rhombohedra have the same ratio as their sectors' volumes, i.e., $\tau:1$.
- ⁴⁵This use of "twelvefold" is contrary to the common sense of "axis of 30° rotations" [e.g., the twelvefold NiCr quasicrystal of T. Ishimasa *et al.* *Phys. Rev. Lett.* **55**, 511 (1985)].
- ⁴⁶I will reserve the terms "(first) neighbor" and "bond" for the results of a Voronoi construction.
- ⁴⁷If we arbitrarily resolved the ambiguity of the Voronoi construction by including one bond across each octahedron to divide it into tetrahedra, we would get $Z=14$ in place of (14). (This procedure also gives $Z=14$ in an fcc lattice.)
- ⁴⁸Diagrams of the neighbor shells of all 24 3D PT vertices and all 21 "twelvefold" superstructure sites are available from the author.
- ⁴⁹(a) The numerical values of Table III are *not* quite raw output. The computer program actually used the count of all b separations (including \tilde{b} second neighbors) in classifying vertices. Fortunately, as one sees in Table IV, each combination $(\alpha, \beta + \tilde{\beta}, \gamma)$ has only one possible identification as $(\alpha\beta\gamma\tilde{\beta})$. (b) The twelvefold vertices are a subset of the basic 3D PT but the τ^2 inflation includes some vertices which are not part of it [V. Elser (private communication) and D. Levine (private communication)]. Furthermore, as I noted in Sec. III A, the twelvefold subset has diffraction spots in the same places in Fourier space as the basic 3D PT does (with a different pattern of intensities, of course). But the τ^2 inflation has a diffraction pattern smaller by a factor τ^2 , which means that the "odd" spots will be in different positions (see Ref. 5).
- ⁵⁰For the $l=1, 5$, and 10 chains, we can consistently break the ambiguity in the site-vacating rules by splitting the sector along its symmetry axis and including only one of the halves in \mathcal{S}_1 .
- ⁵¹V. Elser (unpublished).
- ⁵²This definition of " α " differs from that of Sec. III: in both cases " α " neighbors are counted, but now only those which are twelvefold sites.
- ⁵³N. D. Mermin and S. M. Troian, *Phys. Rev. Lett.* **54**, 1524 (1985).
- ⁵⁴P. Bak, in *Scaling Phenomena in Disordered Systems*, edited by R. Pynn and A. Skjeltorp (Plenum, New York, 1986); *Phys. Rev. Lett.* **56**, 86 (1986).
- ⁵⁵M. V. Jarić, *Phys. Rev. Lett.* **55**, 607 (1985).
- ⁵⁶D. Mercier and J. C. S. Levy, *Phys. Rev. B* **27**, 1292 (1983). (Note that my "radial distribution function" is their "pair distribution function;" they use the former term with a different meaning.) See also J. C. S. Levy, *J. Phys. (Paris)* **46**, 215 (1985).
- ⁵⁷V. Kumar, D. Sahoo, and G. Athithan (unpublished).
- ⁵⁸D. Frenkel, C. L. Henley, and E. D. Siggia (unpublished).
- ⁵⁹J. E. S. Socolar and P. J. Steinhardt (unpublished).

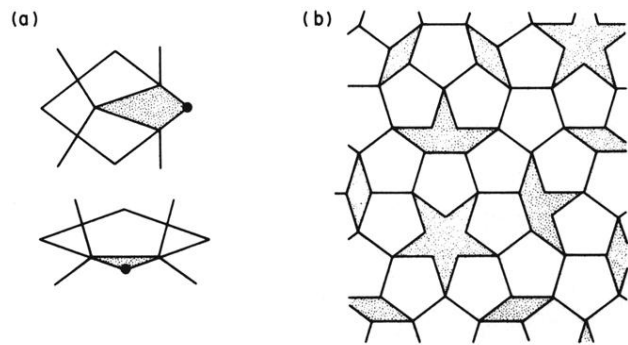


FIG. 7. Pentagon packing on the 2D PT. Decorating Penrose rhombohedra as in (a) (the dots indicate the "pole" vertices here) generates the packing shown in (b).

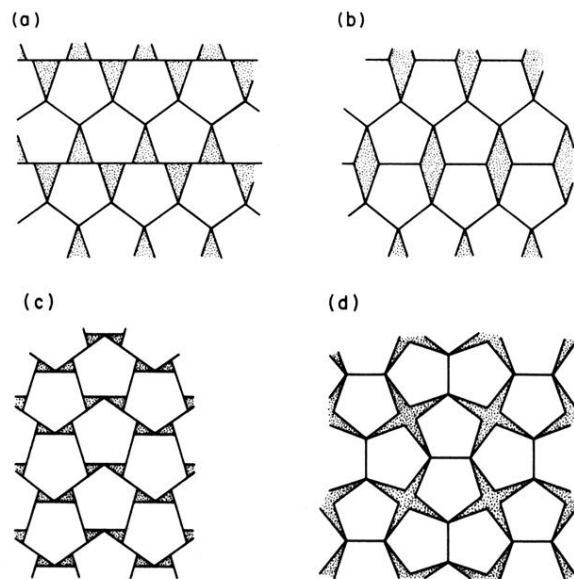


FIG. 8. Crystalline packings of pentagons. Packing fractions: (a) and (b), 0.854; (c), 0.921; (d) 0.828.